



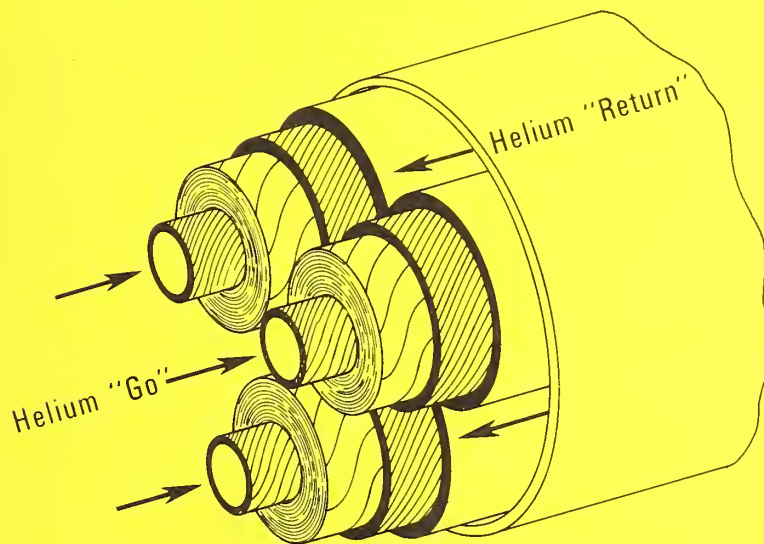
A11104 551582

NBSIR 79-1618

HELIUM RESEARCH IN SUPPORT OF SUPERCONDUCTING POWER TRANSMISSION

ANNUAL REPORT

(October 1977-September 1978)



Prepared by

THERMOPHYSICAL PROPERTIES DIVISION
NATIONAL BUREAU OF STANDARDS
BOULDER, COLORADO 80303

Prepared for

BROOKHAVEN NATIONAL LABORATORY
POWER TRANSMISSION PROJECT
UPTON, NEW YORK 11973

QC
100
.U56
79-1618
1979

HELIUM RESEARCH IN SUPPORT OF SUPERCONDUCTING POWER TRANSMISSION

Annual Report for the Period
October 1, 1977 - September 30, 1978

Prepared by
Thermophysical Properties Division
Center for Mechanical Engineering and Process Technology
National Bureau of Standards
Boulder, Colorado 80303

D.E. Daney, Editor
Contract No. 433475-S

Prepared for
Brookhaven National Laboratory
Power Transmission Project
Upton, New York 11973



U.S. DEPARTMENT OF COMMERCE, Juanita M. Kreps, Secretary

Luther H. Hodges, Jr., Under Secretary

Jordan J. Baruch, Assistant Secretary for Science and Technology

NATIONAL BUREAU OF STANDARDS, Ernest Ambler, Director

CONTENTS

	Page
1.0 THERMAL CYCLE TESTS OF MODEL CABLE.....	1
1.1 Introduction.....	1
1.2 Experimental Apparatus.....	1
1.2.1 Instrumentation.....	5
1.2.2 Test Procedure.....	8
1.3 Cable Clamp Assembly Procedure.....	9
1.4 Results and Discussion.....	13
1.4.1 Cable One.....	13
1.4.2 Cable Two.....	15
1.4.3 General Discussion.....	18
2.0 CABLE COOL-DOWN EXPERIMENTS.....	23
3.0 COOL-DOWN COMPUTATIONS.....	26
Cool-down of Superconducting Power Transmission Lines with Single Phase Helium (paper presented at the 71st Annual Meet- ing of AICHE, Miami Beach, Florida, Nov. 12-16, 1978).....	1

During FY 78, the NBS Thermophysical Properties Division program of supporting research for Superconducting Power Transmission Line (SPTL) development focused on three tasks:

- 1) Numerical computation of SPTL cool down by both single stream and counter flow methods
- 2) Experimental modeling of counterflow SPTL cool down
- 3) Thermal cycling of lengths of lead-sheathed model cable destined for testing in the BNL 5th Ave. facility.

The preparation of computer codes and numerical computation of SPTL cool down were completed and the results are given in Section 3. These calculations confirm our original intuitive judgment that cool-down times for the counterflow arrangement can be long - twenty days or more.

Greater than anticipated computer run times and costs required a reduction of effort on experimental modeling of counterflow cool down. Consequently, completion of this task will be delayed until FY 79.

Two sections of cable underwent extensive thermal cycling, and the results of these tests are given in Section 1. The complex structure of the cable leads to unusual (although reproducible) load vs time curves.

Funding limitations required postponement until FY 79 of the experimental evaluation of heat flow sensors as a means of non-intrusive vacuum indication for SPTL vacuum envelopes. This task together with experimental modeling of cool down will form the heart of our program in FY 79.

Key words: Cable cool-down; cool-down helium; liquid helium; superconducting power transmission, thermal cycling, thermal stress.

1.0 THERMAL CYCLE TESTS OF MODEL CABLE

(C. F. Sindt and P. R. Ludtke)

1.1 Introduction

The goal of these tests was to investigate the thermo-elastic behavior of a 3.5 meter section of BNL model cable while the cable is subjected to repeated thermal cycles between ambient temperature and operating temperature. In practice, the ends of the SPTL cable will be fixed (i.e., the length of the cable held constant) so that a significant thermally induced axial stress will develop in the cable as it is cooled.

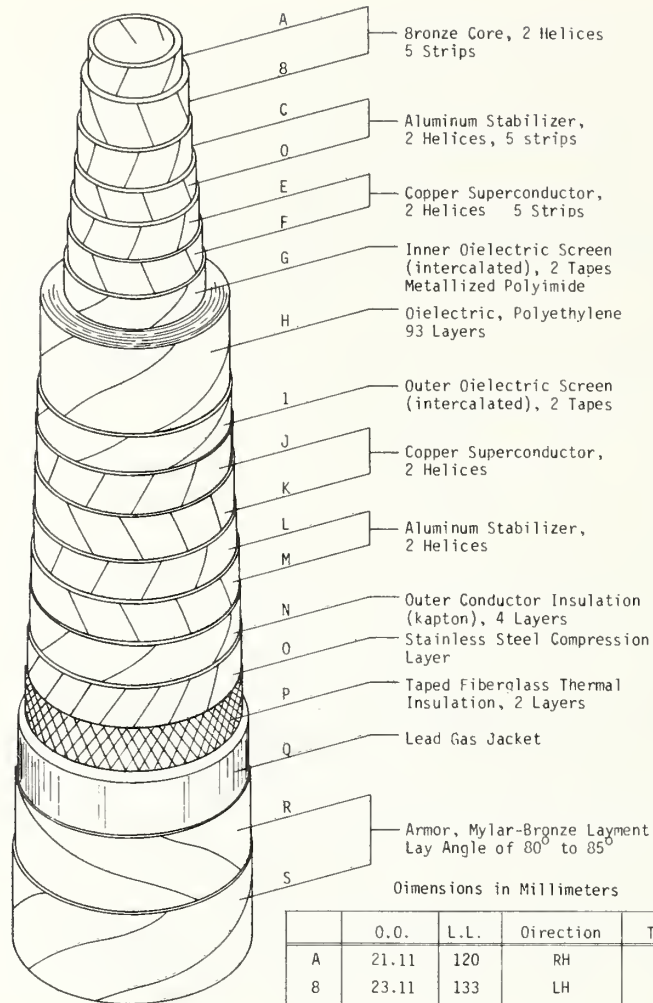
The cable is built up from a number of helically wrapped layers (bronze core, superconductor, dielectric), one of the outer layers being a lead sheath which provides a hermetic seal (see figure 1.1). The cool-down tensile load produces an elastic deformation in the helically wound elements which act as coil springs. If friction between these elements is neglected, then this spring load is small compared to the load on the lead sheath, which is stressed beyond its elastic limit during cool-down. Likewise, the lead sheath will be compressed beyond the elastic limit during warm-up. Although repeated thermal cycling of an operating SPTL is not expected, it is nevertheless necessary to provide for this contingency. Thus the cable must remain functional throughout a number of thermal cycles.

In these tests, two different 3.5 m lengths of cable were subjected to a number of thermal cycles while maintaining the cable length constant. The primary test objective was to observe if physical damage to the cable would occur as a result of thermal cycling. Additional objectives were: to determine the cable tensile and compressive loads during thermal cycling; to test the ability of the end clamps to withstand thermal and assembly cycles; and to determine if the cable or end clamps developed leaks at operating temperature and pressure.

1.2 Experimental Apparatus

The test fixture, figures 1.2 and 1.3, must meet several requirements in these constant length thermal cycling tests: 1) it requires a mechanism for maintaining the cable length constant with varying load; 2) it requires a dewar and cryogenic fluid system for cooling the cable to LN₂ temperature (77 K); and 3) it requires a gripper and seal arrangement to transmit load from the cable to the test fixture while maintaining a hermetic seal with the lead sheath.

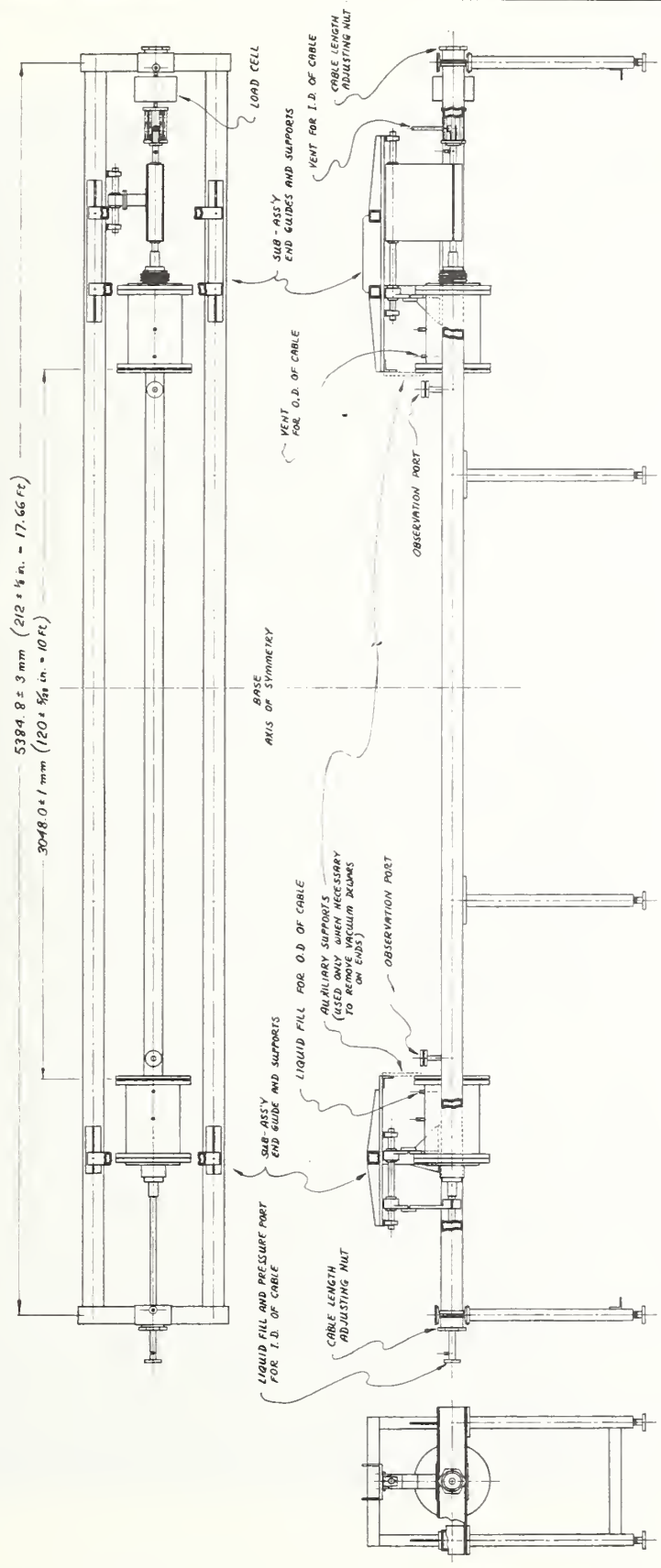
The test fixture, which accommodates a cable segment, has a rectangular steel framework built up from two 100 mm square tubes 5.4 m long that are bridged at each end by 75 x 127 mm H beams, 0.5 meters long. A screw mechanism at each end may be manually adjusted so as to maintain the cable



Dimensions in Millimeters

	O.O.	L.L.	Direction	Thickness
A	21.11	120	RH	1.02
B	23.11	133	LH	1.02
C	23.88	89	RH	.38
D	24.64	36	LH	.38
E	24.84	112	RH	.10
F	25.04	112	LH	.10
G	25.15		RH	.20
H	40.38			7.62
I	40.48		LH	.05
J	40.69	185	RH	.10
K	40.89	185	LH	.10
L	41.65	157	RH	.38
M	42.41	157	LH	.38
N	43.43		RH	.51
O	44.45	229	RH	.51
P	45.46			.51
Q	49.79			2.16
R	50.14			.178
S	50.50			.178

Figure 1.1 Cable cross section, cut back view



NATIONAL BUREAU OF STANDARDS		OCTOBER, 1977	
THERMOCYCLING TEST APPARATUS		SHEET 1	
PROJECT		SCALE 1/8" = 1"	
DRAWN BY		CHECKED BY	
DESIGNED BY		APPROVED BY	
DATE		DATE	
BY		BY	
FOR		FOR	
275		/05	

Figure 1.2 Cable test apparatus

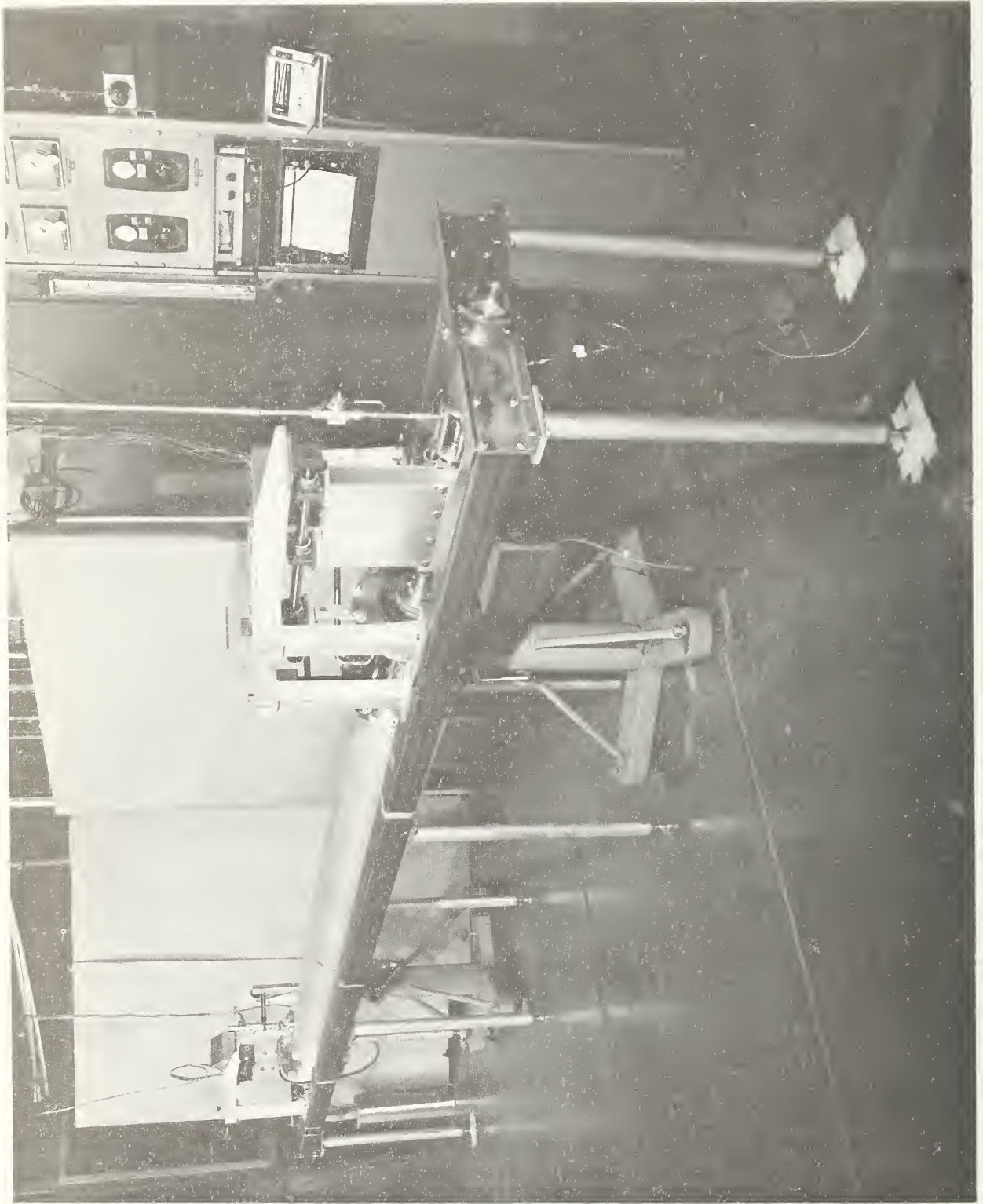


Figure 1.3 Photo, cable test apparatus

length constant in the face of variable loads. The cable is enclosed in a polyurethane foam insulated spool piece (74 mm ID) and the end clamps are enclosed in the vacuum insulated housings at each end. The cable, spool piece and end housings are all supported at either end by rails with linear ball bearings, figure 1.4.

The cable assembly is isolated from forces in the support structure by means of internal and external bellows in the end housings, as well as by means of O-ring slip joints at the end housings, figure 1.5.

1.2.1 Instrumentation

The length of the cable is monitored with 30 power microscopes which are aligned with view ports 86 mm from each end of the spool piece. These microscopes are supported from the concrete floor by heavy duty tripods, so their position is independent of the load on the cable and test fixture. The cable length reference points are scribe marks on invar rods which are attached to the end fixtures. The cable length was held constant to within ± 0.12 mm using this system of microscopes and adjusting screws.

Cable temperatures were determined with type T thermocouples referenced to a boiling liquid nitrogen bath. For the first cable segment tested temperatures were measured at three positions: at the axial midpoint on the lead sheath, at the load cell end of the bronze core, and 15 mm into the wrapped dielectric.

For the second cable segment tested, a single thermocouple was mounted in the wrapped dielectric at the load cell end. The uncertainty in the measured temperatures is estimated to be less than 1 K.

The cable was cooled from one end rather than uniformly along its length, so the purpose of these temperature measurements was to determine when the entire cable segment had cooled to the desired temperature. The measurements were not intended to represent the temperature of the cable composite since the sensor could not be placed in the body of the cable without destroying the integrity of the lead sheath.

The axial tensile or compressive load on the cable was determined with a load cell (9000 N (2000 lb) capacity). A purely axial load at the cell is assured by the guide mechanism for the cable extension tube shown in figure 1.4. The calibration accuracy of the load cell is .25 percent of full scale (2000 pounds). The precision of the load cell was checked with class S weights; the measurement uncertainty was 0.1 percent.

The axial load on the cable due to external forces differs from the force on the load cell and is given by the expression

$$F_c = F_d + F_p \pm F_f \quad (1)$$

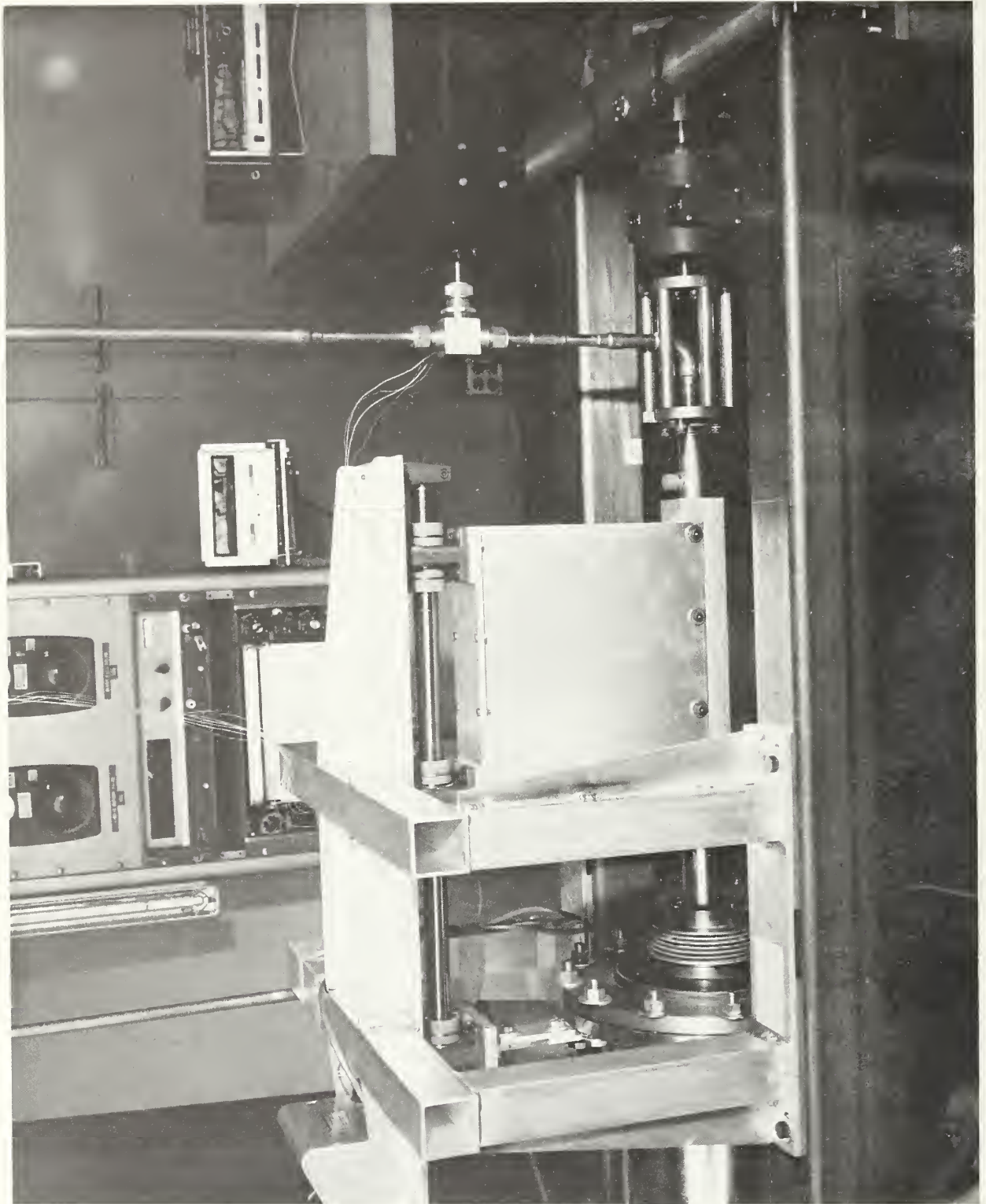


Figure 1.4 Load cell end, test apparatus

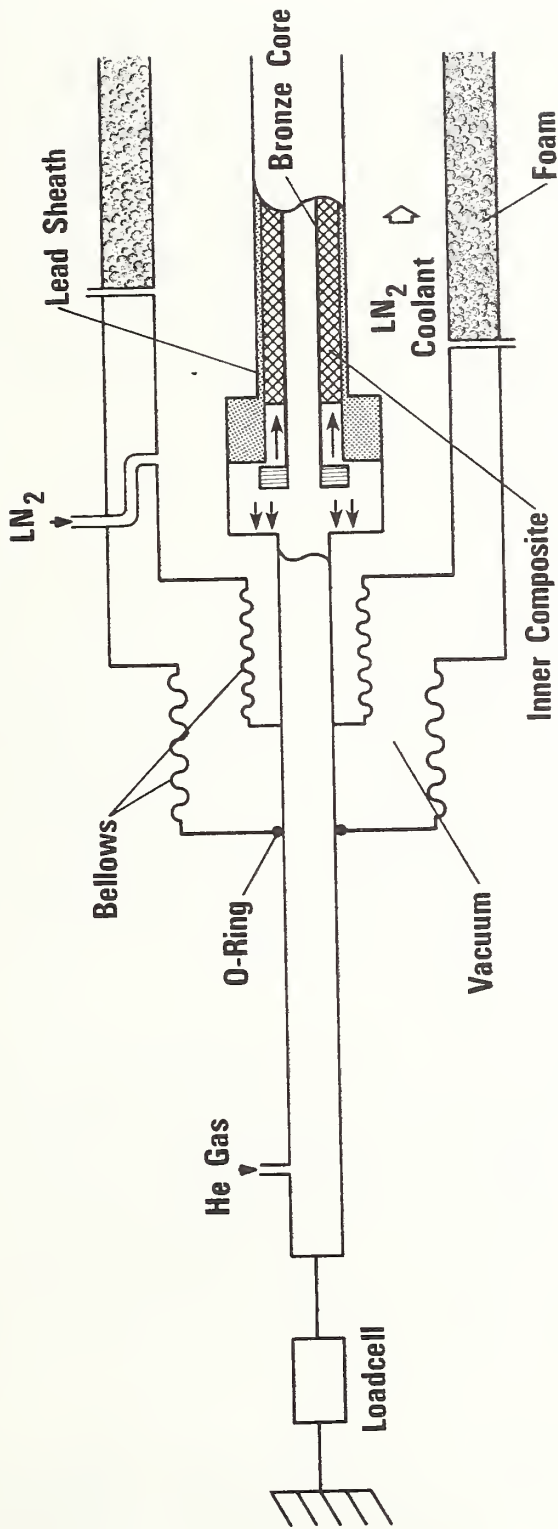


Figure 1.5 End assembly schematic

where F_c is the force on the cable, F_d is the force measured by the load cell, F_p is the pressure force due to the differential pressure across the end fixtures, and F_f is the friction force on the cable and cable extensions. The friction force from the supports and O-ring seal is estimated to be less than ± 45 N (± 10 lbs)--small compared to the other forces. The pressure force, F_p , is due to the differential pressure across the inner bellows assembly. A tensile force of 151 N (34 lbs.) results.

In considering the effect of internal pressurization of the cable, we note that the behavior of a composite cable can be much less predictable and reproducible than the behavior of a noncomposite cable. Referring to figure 1.5, the axial force on the composite cable due to internal pressurization is approximately

$$F_{cp} = P [A_s - (A_s - A_c) (1 - \alpha)C] \quad (2)$$

where P is the differential internal pressure, A_s is the inside area of the lead sheath, A_c is the inside area of the bronze core, α is the void fraction of the composite inside the lead sheath, and C is the degree of coupling between the inner composite and the lead sheath and clamp assembly. For complete coupling ($C=1$) and zero porosity equation 2 gives the pressurization force on the cable as that for a heavy wall tube with inside area A_c . For zero coupling, the force is that for a thin walled tube with inside area A_s . For an internal cable differential pressure of 1.5 MPa, F_{cp} may vary from 2470 N (555 lbs.) to 340 N (77 lbs.), depending on the voids in the inner composite and the degree of coupling between the lead sheath and the inner composite.

Another important consideration is the effect internal pressurization has on the spring constant of the various metal helices in the cable. The bronze core and other metal helices may exert axial forces as a result of temperature change, and these forces may change as the result of internal pressurization. This is because the various helices behave as springs in the absence of friction, but could tend to behave as rigid tubes if there is friction between them. Such friction could decrease if the lead sheath were pushed radially away by pressure, or increase if the sheath contracted more than the rest of the cable during cooldown.

1.2.2 Test Procedure

Two cable samples were tested, each by a different procedure. Cable one was cooled and then pressurized, whereas cable two was cooled with the cable interior pressurized. The latter procedure simulates the expected operating conditions more closely.

Cable one was first leak checked by pressurizing the cable interior with helium gas to 1.5 MPa and measuring the rate of pressure decay in the valved-off system over a 15 minute period. The sensitivity of the pressure measurement was 3.4 kPa. All pressurization and depressurization cycles were made in 345 kPa increments, so that the cable could be maintained at a fixed length by means of the adjusting screws.

After the leak check, the pressure was bled down to ambient pressure and the cable was cooled to liquid nitrogen temperature by flowing LN₂ through the bronze core and around the outside of the cable. The LN₂ flow rate was adjusted so as to achieve cool-down in about 90 minutes. The cable was then again leak checked by measurement of the pressure decay using helium gas prechilled to about 80 K. Following the leak check, the cable interior was bled down to ambient pressure (again in 345 kPa increments to allow for cable adjustment) and the cable was warmed by flowing 350 K nitrogen gas through and around it. The cable warmed to 200 K in about 3 hours. The remainder of the warm-up was achieved unattended in the following 12 hours using a low flow rate of ambient temperature nitrogen gas.

The procedure for cable two was the same, except it was cooled down with the interior pressurized to 1.5 MPa. Cable one was cycled 20 times and then removed for inspection. Cable two was cycled 5 times, removed for inspection, then reassembled and cycled an additional 15 times.

Both cables were preloaded with 590 N (134 lbs) tension (440 N, 100 lbs, load cell and 150 N, 34 lbs, bellows force) before the first thermal cycle. The cable length was then referenced by fixing the microscope cross hairs on the scribe marks of the invar rods, and this length was maintained throughout the test series.

1.3 Cable Clamp Assembly Procedure

Because the cable clamp assembly procedure may be of interest in its own right, we have included it here in some detail. The lead seal and terminal clamp assembly for attaching the end of the cable to the test fixture was provided by BNL. An enclosure cap was added to the clamp assembly, as shown in figure 1.6, to facilitate pressurization of the inner line and to provide the structural link between the cable and the test fixture.

The clamp assembly was installed as instructed by BNL. Two layers of nylon filament tape were wrapped over the mylar-bronze wrap of the cable for the 76 mm length covered by the flexible end of the outer clamp assembly. After positioning the outer sleeve assembly, an aluminum ring was slipped over the flexible end while a regular hose clamp compressed the flexible fingers. The sleeve assembly O.D. was 60.3 mm (2.375") and the ring I.D. was 59.8 mm (2.356") x 19 mm wide. In addition to the ring, a regular hose clamp

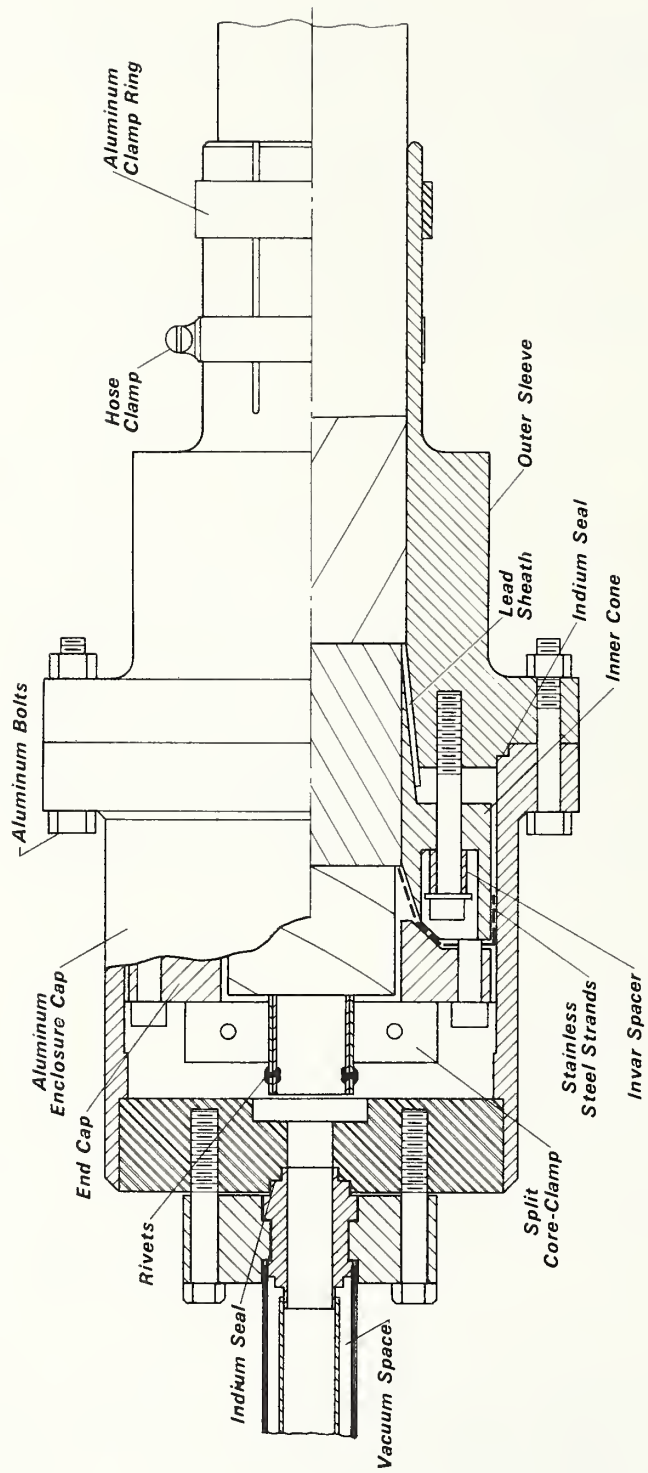


Figure 1.6 Lead seal/terminal clamp assembly

was also used midway on the flexible end. It was impossible to use the clamp provided by BNL because there was insufficient room in the test fixture spool piece for the clamp.

After securing the outer sleeve assembly, specially prepared tools with well-rounded corners were used to form the lead into a cone shape against the outer sleeve. Extreme care was necessary when forcing the inner cone inside the lead sheath; it was very easy to score the lead with the sharp leading edge of the inner cone. The inner cone was drawn into position with the bolts used to connect it to the outersleeve. The bolts were evenly tightened to keep the cone and sleeve flange faces parallel. The inner cone bolts were retightened 3 to 5 times after relaxation periods of 3 hours to allow the lead to flow between the cone-shaped enclosure.

Next, the stainless steel strands were pulled tight across the back of the inner cone and bent sharply around the outer corner in the inboard direction. The ends were clamped flat against the outside of the inner cone piece with metal clamps. The end cap was then bolted securely to the back of the inner cone clamping the stainless steel strands, while maintaining uniform spacing between the end cap and inner cone.

A solid copper wire of 1.6mm diameter was tapped in between the end cap and the stainless steel strands in order to keep the 90° corner of the stainless steel strands tight against the inner cone corner. The metal clamp around the ends of the strands was then replaced with two layers of nylon filament tape, thus securing the ends of the stainless steel strands to the O.D. of the inner cone, as shown in figure 1.7.

A split clamp 1.3 cm thick, was then bolted together around the inner bronze core. One side of the split clamp fit flat against the end plate and the opposite side was machined to fit just inboard of the rivets securing the inner bronze core (2 helices). The split clamp was used to complete the structural link between the bronze inner core and the clamp assembly, thus incorporating the bronze core as a structural member when the cable incurs tensile stress, i.e., the clamp transmits only tension forces from the bronze core to the end cap.

An enclosure cap was then bolted to the outer sleeve flange with aluminum bolts. Aluminum bolts rather than stainless steel were used to eliminate a differential contraction seal problem. Indium wire of 1.5 mm diameter was used to seal the cap to the outer flange. A special step design with close tolerances was used to trap the indium. The spacing between the flanges was maintained uniform while tightening the bolts. The flange bolts were retightened several times after 3 hour periods to allow indium flow and subsequent relaxation of the bolt stress.

A 25 mm O.D. stainless tube was then bolted to the end of the enclosure cap using the same type of indium seal. This support tube completed the

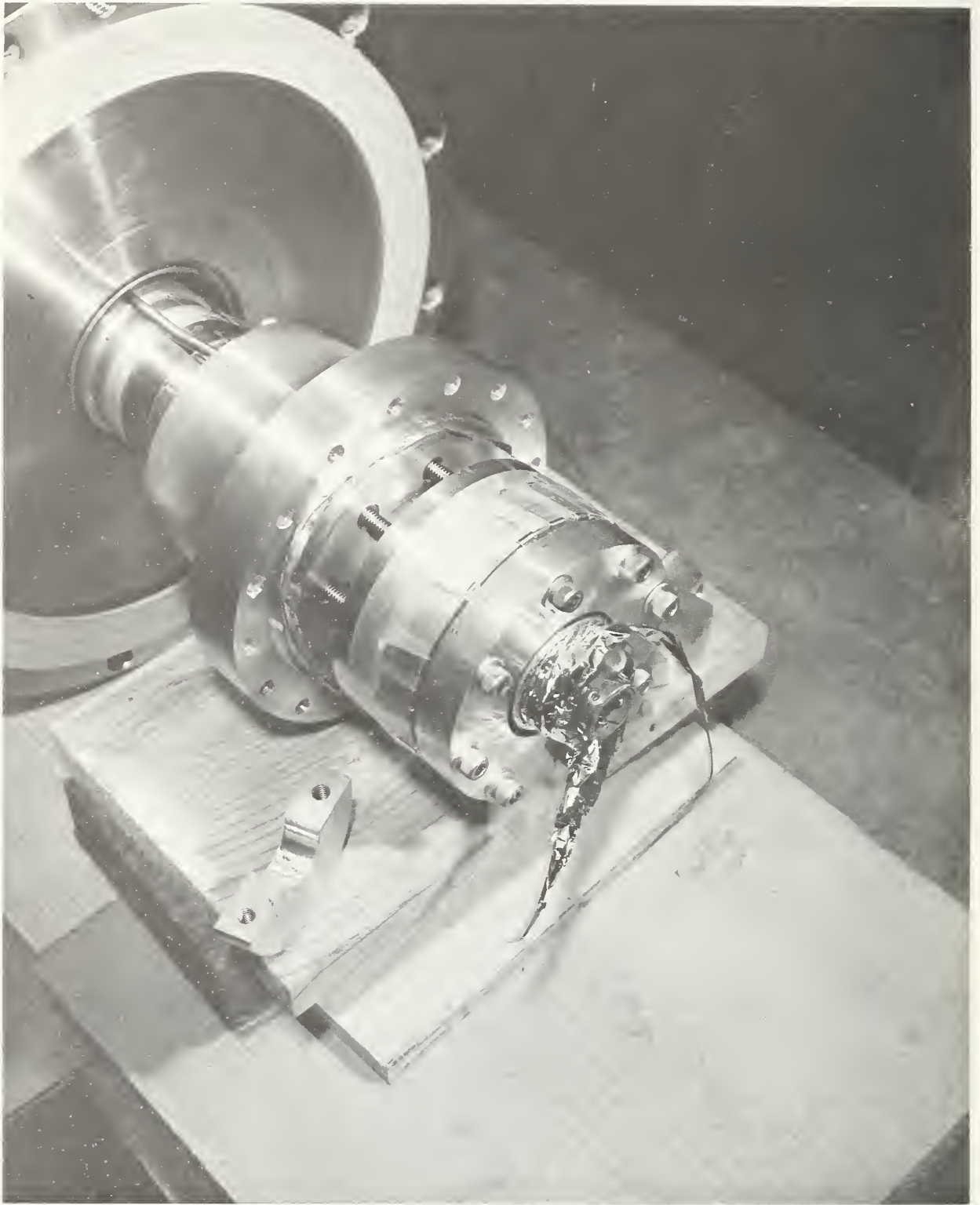


Figure 1.7 Photo, lead seal/terminal clamp

enclosure of the inner line and served as the structural member between the cable ends and the test apparatus.

Disassembly of the clamp was quite straightforward, except care was required in removing the inner cone and outer sleeve from the cable. Removing the inner cone was accomplished by using 3 pieces of thread stock with nuts and washers between the inner and outer cone pieces. The nuts were adjusted to slowly force the cones apart. Hammering at the inner cone or prying between the two would damage the stepped seal surfaces. Once the lead sheath is separated from the inner cone, the cone slides off freely.

Removing the outer sleeve from the cable also requires care. It is possible to exert sufficient force on the outer sleeve to cause yielding of the entire lead sheath inboard from the clamp. In order to remove the outer sleeve with minimal force, the lead must be carefully worked away from the outer cone with a rounded tool. Separating the lead from the outer sleeve significantly reduces the force required to swage the lead back to a cylindrical shape while removing the outer sleeve.

The lead seal clamp assembly worked very well during the two twenty-cycle test periods; each clamp was installed and removed three times. The assembly functioned well as a cable terminator, with no damage to the cable ends. There was no significant leakage during the entire test period.

1.4 Results and Discussion

1.4.1 Cable One

Figure 1.8 presents load cell vs. time for four typical thermal cycles of the 20 cycles to which cable one was subjected. The test data is constrained to definite time intervals, i.e., actual cool-down time may have varied slightly (\pm 10 minutes) from the 1-1/2 hours indicated. Following the first thermal cycle, the preload on the cable changed from the initial 440 N (99 lbs) tension (load cell reading) to 1330 N (299 lbs) compression and remained near this value for the remaining 19 tests. This shift in the initial cable (load cell) load occurred with both cables and is attributed to the yielding of the lead sheath which occurs during the first thermal cycle. As the cable is cooled the load passes through a maximum and then decreases slightly as the cable comes to equilibrium at 76 K. This behavior may be due to creeping of the spirally wound core with respect to the lead sheath.

As the cable is pressurized, the load cell force is reduced by approximately 4000 N (900 lbs) compared to the maximum of 2469 N (555 lbs) that we calculate for the pressure x area term. For a solid cable the two forces must be equal. In this case, however, it is likely that pressurizing the lead sheath releases the grip of the sheath on the inner composite sufficiently that the composite relaxes even though its length is held

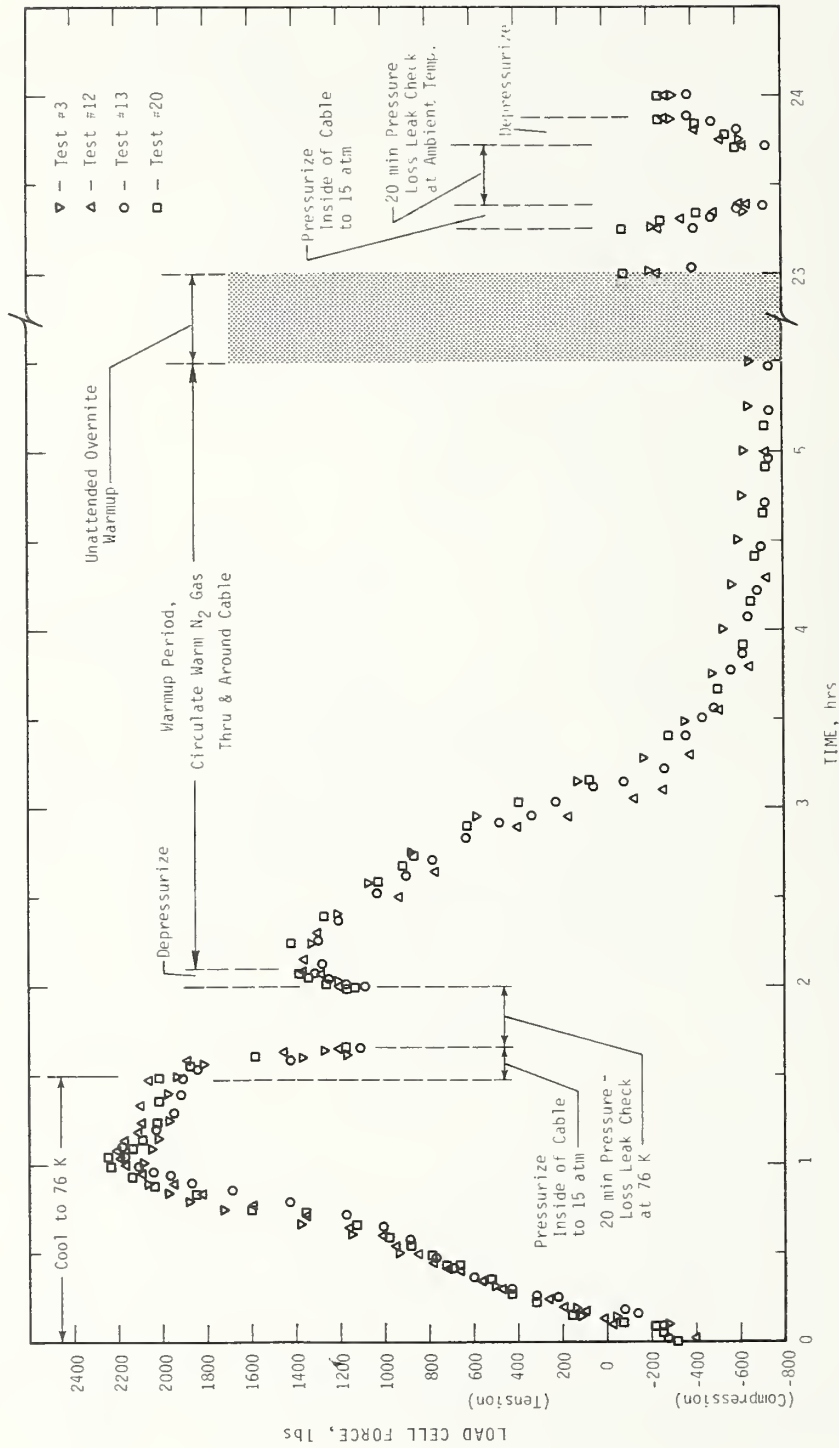


Figure 1.8 Cable 1, thermal cycle test results

constant. A recovery of 800 N (180 lbs) in the tension load occurs as the cable core is depressurized. This is within the range of 343 N (77 lbs) to 2466 N (554 lbs) which may be attributed to the pressure x area term, but differs appreciably from the average change of 1600 N (360 lbs) which occurred when the cable was pressurized for leak checks at ambient temperature. The hysteresis in these ambient temperature pressure cycles was small. The load decreased by 1646 N (370 lbs) with pressurization and increased by 1557 N (350 lbs) with depressurization.

The maximum and initial load cell force for each cycle is given in figure 1.9. As both figure 1.8 and figure 1.9 indicate, the behavior of the cable was consistent from cycle to cycle.

After test number 20, the cable was removed from the test fixture. The enclosure cap and split end cap were removed from the clamp assembly, revealing the end of the cable inside the stainless steel strands. We found that the dielectric and outer dielectric screen had unraveled slightly as shown in figure 1.7. This was probably due to relative movement between the cable layers near the severed end of the cable.

After removing the cable from the centerspool piece, we found that the lead sheath had extruded radially outward between the bronze wrapping, as shown in figure 1.10. This radial bulge or spiral annulism occurred at the end opposite that where liquid nitrogen coolant was introduced. In spite of the spiral annulism the lead sheath remained intact, and there was no leakage in this area. After inspecting and photographing the annulism, the cable was sent to BNL for inspection and evaluation.

1.4.2 Cable Two

In view of the problem with cable one, the test procedure was reviewed and it was decided that cable two should be cooled down under pressure since this is the manner in which the cable will be cooled down in practice. It was also decided to thermal cycle the cable 5 times and then remove it for inspection before completing the full 20 cycle test.

Upon inspection after 5 thermal cycles we found that the lead sheath of cable two had expanded outward slightly at the "windows", where the lead sheath was covered with only mylar. Otherwise the cable looked exactly as when it was installed in the test fixture. We saw this same "window" expansion with cable one.

After consulting with BNL, we reinstalled the cable in the test fixture and continued testing it for another 15 cycles. Again, we found no perceptible damage other than the slight expansion at the "windows", which was noted after the first five cycles, and a waviness in the surface which became noticeable when looking down along the cable.

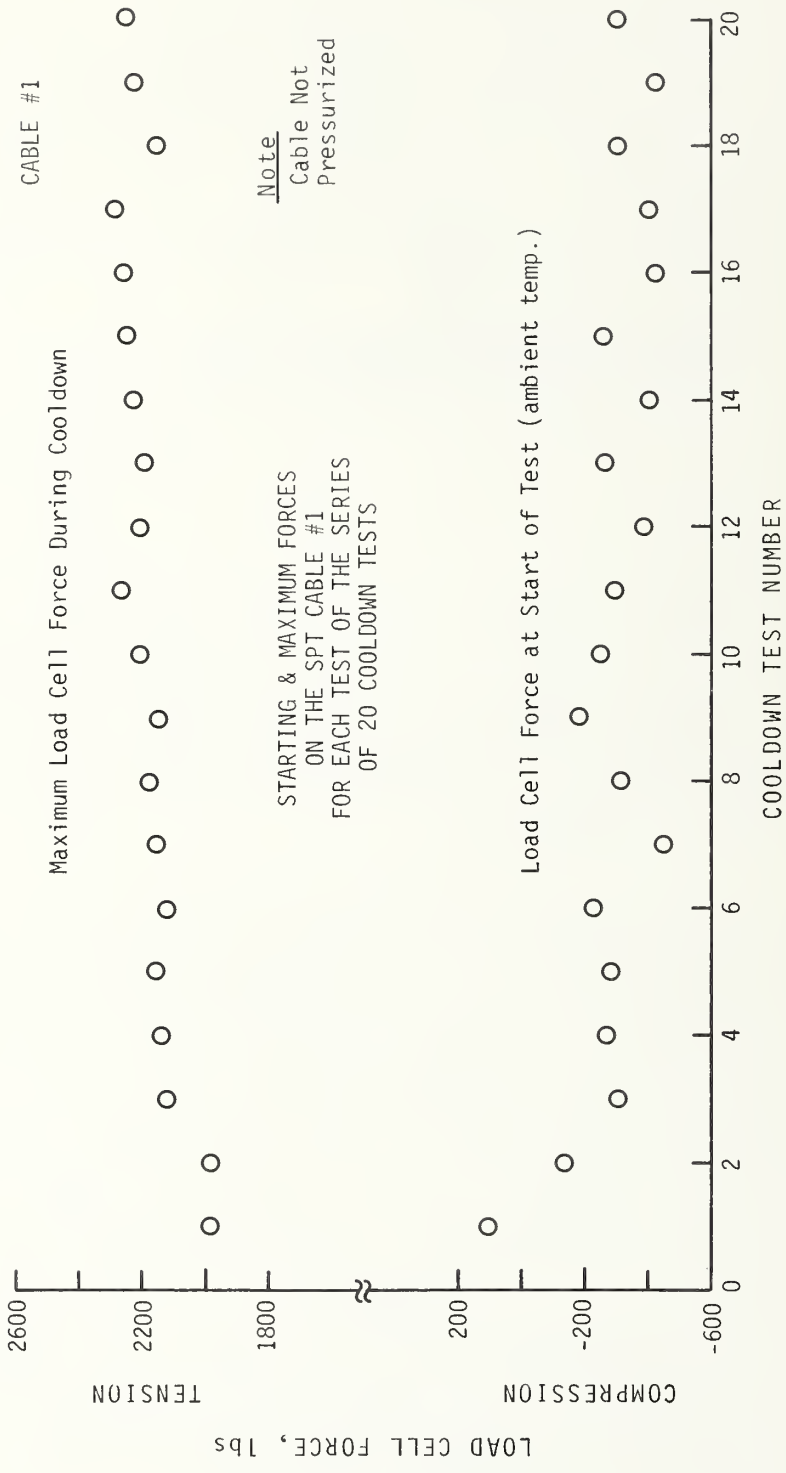


Figure 1.9 Cable 1, starting and maximum forces

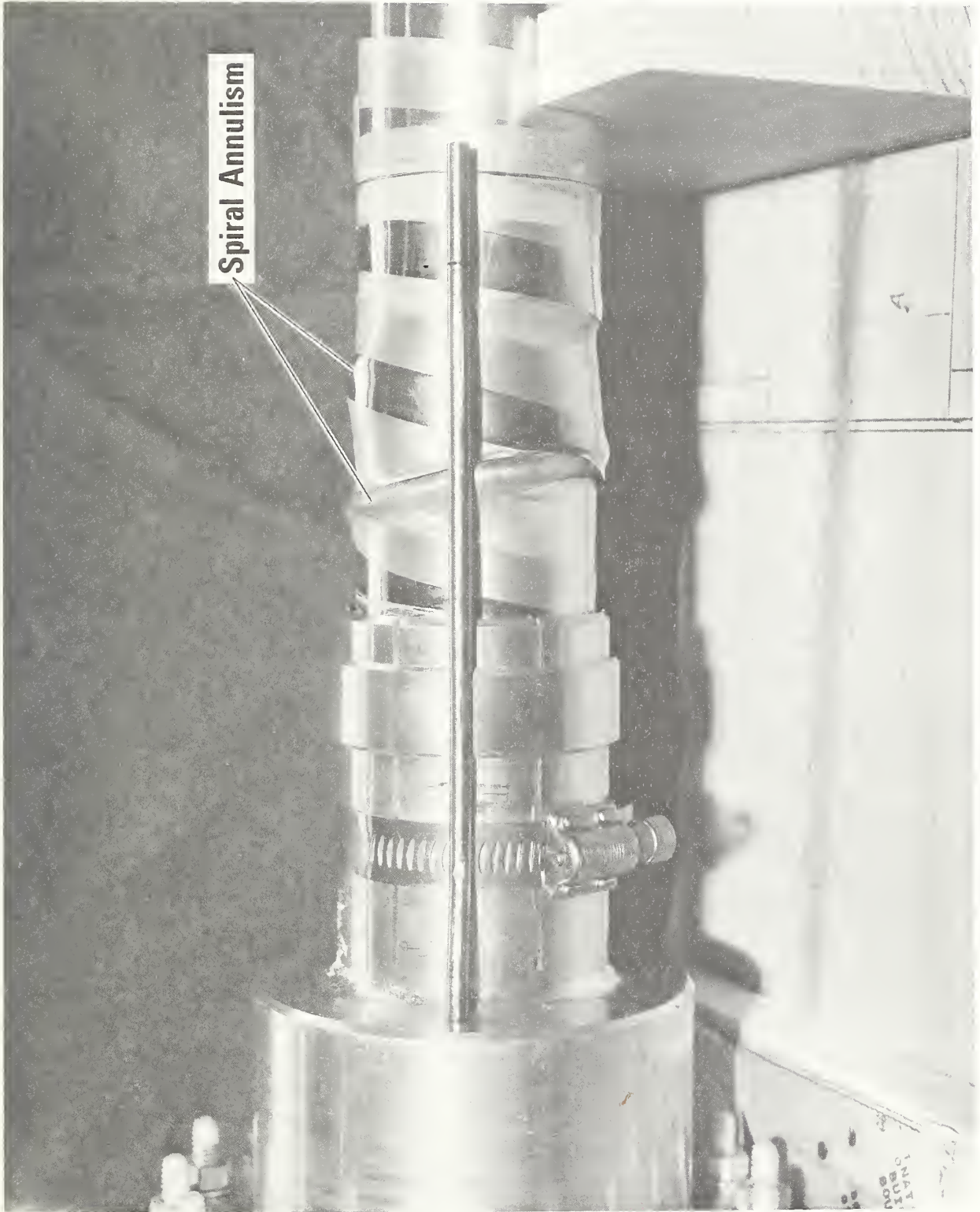


Figure 1.10 Photo, cable 1 lead sheath, annulism

The outside diameter of the cable was measured at random locations along its length, at 90° angles, in order to determine the magnitude of the surface irregularities. From 18 different measured diameters in the two planes, the maximum difference was 1.55 mm (.061 inches). Cable two showed no evidence of the dielectric and outer dielectric screen unraveling or fraying as shown in figure 1.7.

Load cell vs. time measurements for four of the first five cycles is shown in figure 1.11, and data for five of the last fifteen cycles is shown in figure 1.12. The initial and maximum load cell forces for cable two are shown in figure 1.13. As with cable one, the data is quite repeatable.

During a typical test on cable two, pressurization of the inner line (ambient temperature) resulted in a decrease in load cell force of 2220 - 2670 N (500 - 600 lbs) as shown in figures 1.11 and 1.12. During cool-down the load cell force went from approximately 1100 N (250 lbs) compression to 7120 N (1600 lbs) or 7560 N (1700 lbs) tension.

Cable two was then warmed in the same manner as cable one (no internal pressure). The resulting load cell force the next morning, with no internal pressure, averaged 670 N (150 lbs) compression for the first five cycles and approximately 1330 N (300 lbs) for the later 15 cycles, as shown in figures 1.11 and 1.12.

We installed both cables with a tensile force of 440 N (100 lbs) (no internal pressure) but after the first cool-down cycle, this changed to 1110 N (250 lbs) compression on cable one as shown in figure 1.9 and a load cell force of 2670 - 3110 N (600 - 700 lbs) compression on cable two as shown in figure 1.13; the load cell forces given in figure 1.13 are considerably higher than those in figure 1.9 because the cable is internally pressurized.

1.4.3 General Discussion

There was no measurable leakage across the lead sheath during any of the 40 tests. For six of these tests the leak rate was monitored with a wet test flowmeter and for the remainder of the tests the pressure decay method was used.

The cause of the annulism in the lead sheath of cable one is not clear. It could be the result of buckling due to the compressive forces that occur on warm-up. If some yielding due to pressure forces had already occurred at that "window" site then it would be more susceptible to buckling. Whether or not the change in the operating procedure prevented cable two from developing an annulism is problematical, since the mechanism of failure for cable one is unclear. It could be fortuitous that cable one buckled and cable two did not. On the other hand, it is possible that cooling the cable under pressure prevented the annulism by either: a) maintaining tight contact between the lead sheath and the outer mylar-bronze wrapping, thus

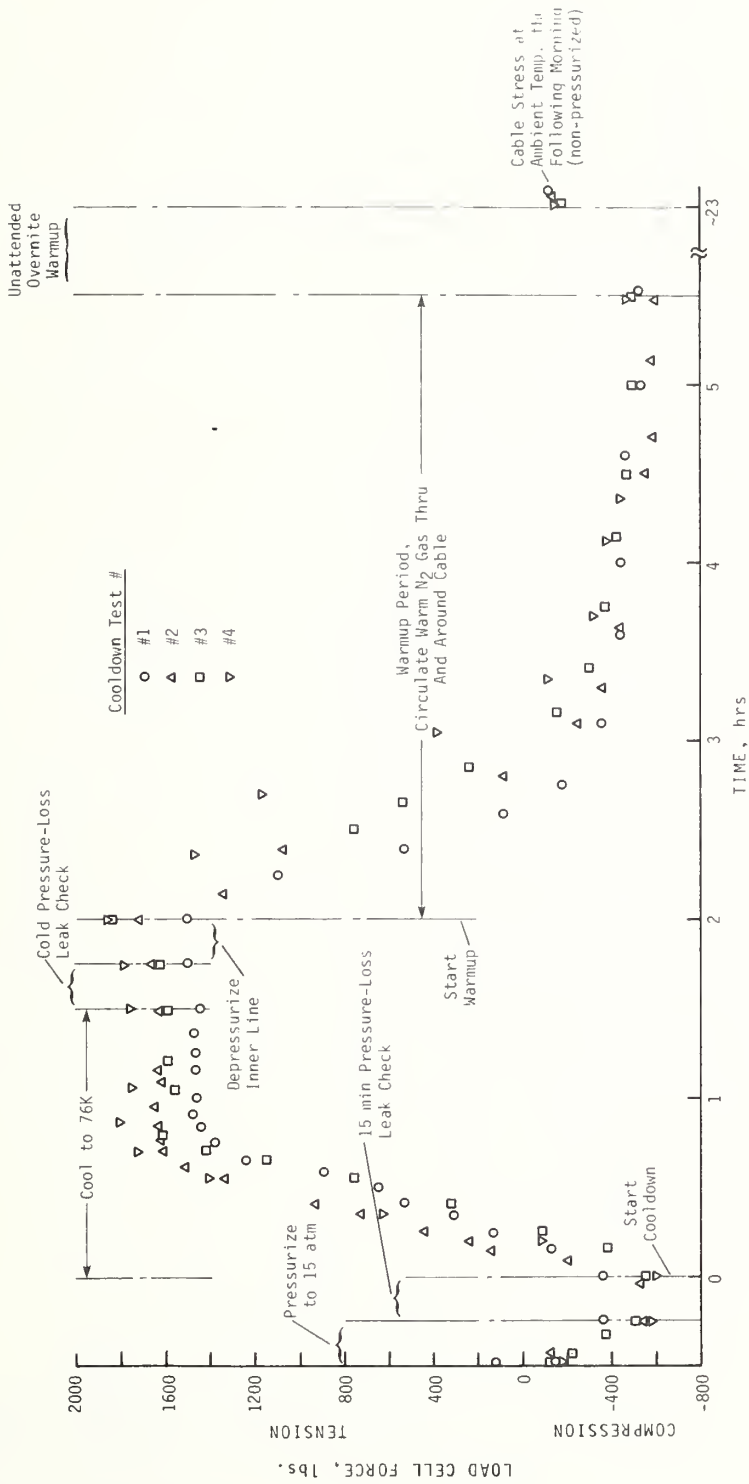


Figure 1.11 Cable 2, thermal cycle test results, first series

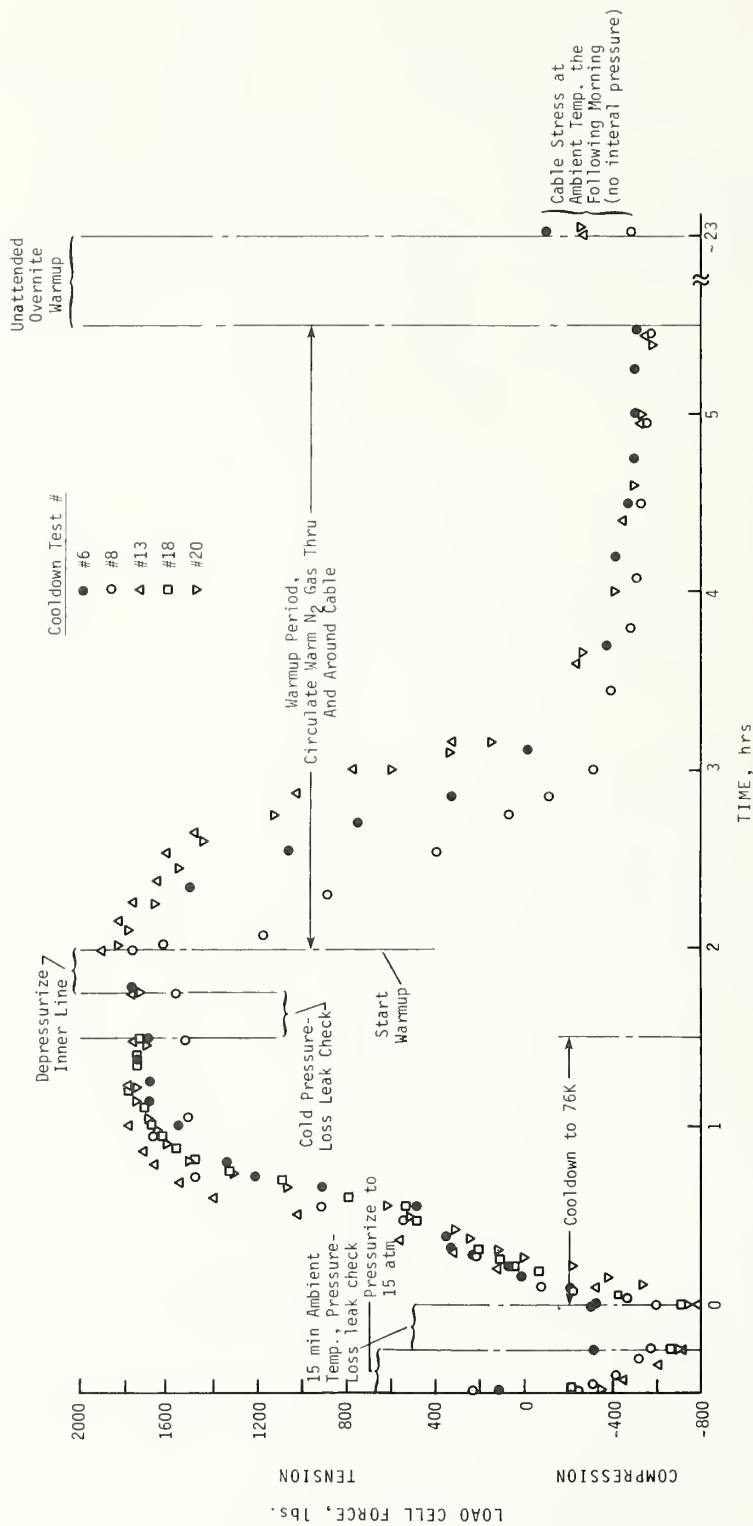


Figure 1.12 Cable 2, Thermal cycle test results, second series

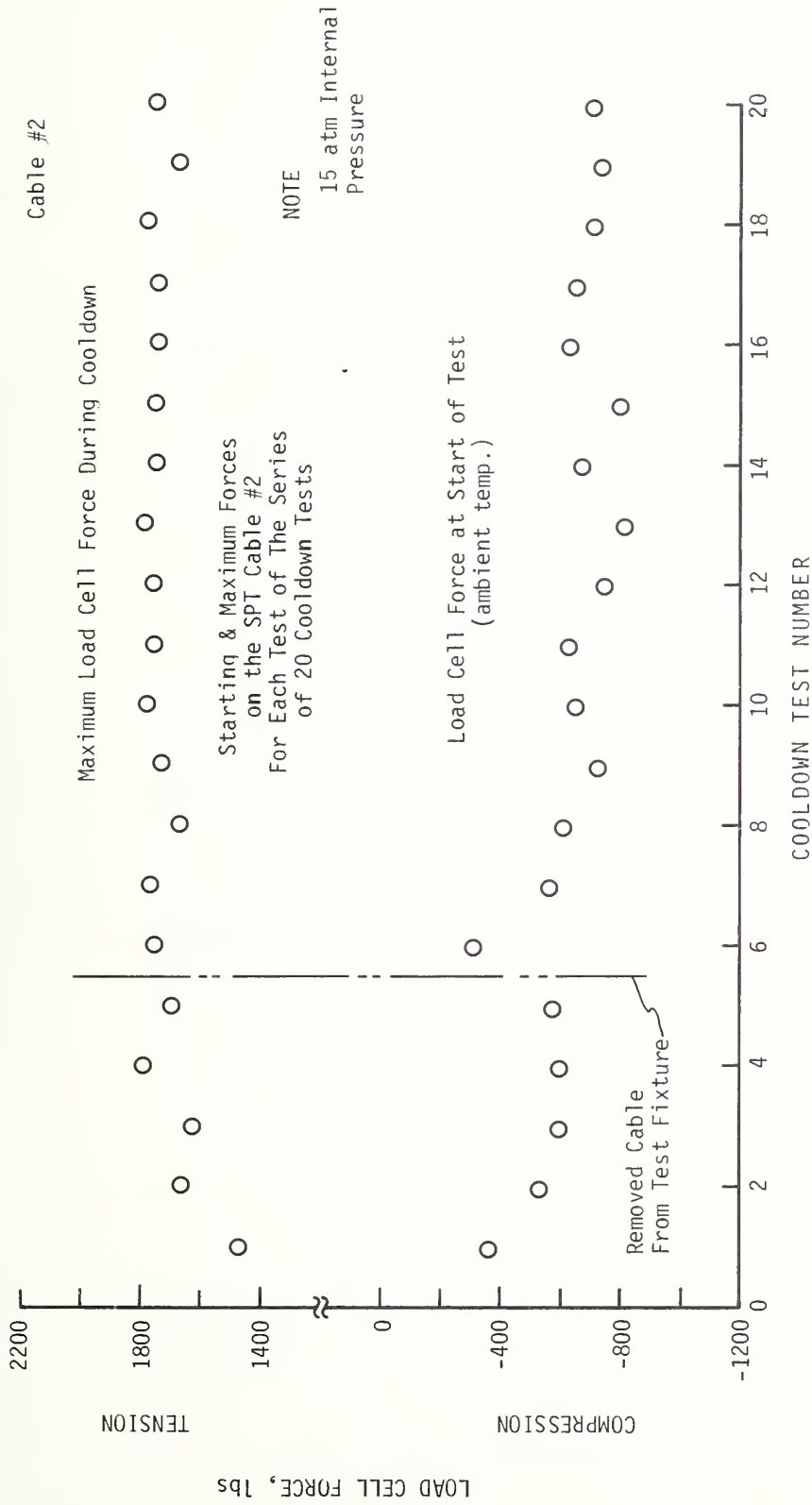


Figure 1.13 Cable 2, starting and maximum forces

preventing relative movement and random enlargement of the window, or b) allowing freer movement of the core with respect to the sheath, and thus reducing the compressive load that the core exerts on the sheath during warm-up.

The thermo-elastic behavior of the cable is quite complex as evidenced by figures 1.8, 1.11 and 1.12. In particular, note the change in load cell force as the cable is pressure cycled between 0.1 and 1.5 MPa, summarized in table I.

Table I. Effect of Cable Pressure on Load Cell Reading

	Change in load cell force, N (lbs)	
	Cable 1	Cable 2
Warm		
Pressurize to 1.5 MPa	- 1650 (- 370)	- 2220 to 2670 (- 500 to -600)
Depressurize to 0.1 MPa	+ 1560 (+ 350)	
Cold		
Pressurize to 1.5 MPa	- 4000 (- 900)	
Depressurize to 0.1 MPa	+ 800 (+ 180)	+ 440 (+ 100)

Without a detailed stress analysis of the complex cable structure, we can do little more than speculate on the cause for such differences in the change in the load cell force. It would seem clear, however, that the thermal-pressure history, and how this history affects the coupling between the lead sheath and the inner composite has a large effect on the force transmitted from the cable to the fixtures.

2.0 CABLE COOL-DOWN EXPERIMENTS

(D. E. Daney)

The time required to cool down a superconducting power transmission line is critical to the success of these lines since excessive cool-down or warm-up times would result in unacceptable long interruptions of service when repairs are required. For example, Jones (section 3.0) has calculated a cool-down time of 20 days for a 15 km line cooled by a two stream counterflow method.

The aim of the cool-down experiments is to model the cool down of counterflow cooled SPTL's such as the ones currently under consideration at BNL and LASL. The two principle goals are to complement the numerical cool down calculations (section 3.0) by providing an empirical test of their validity, and to provide an empirical base for a general theory of counterflow cool down.

The details of the experimental approach are given in our last annual report [1]. To briefly summarize this approach, we are modeling the transmission line with special dual-passage heat exchange tubing which has a controlled thermal resistance (1 mm thick x 9 mm wide stainless steel web) between the two flow channels. This webbing simulates the thermal resistance, which is due primarily to the dielectric, of the prototype cable. Analysis of the cool-down problem indicates the model and cable should have the same value of NTU (number of heat exchanger transfer units) for similar cool-down behavior.

During the past year the work on the cool-down experiment has proceeded at a rather low level so that the cool-down calculations and cable thermal cycling tests could be completed. In FY 79 the cool-down experiments will receive top priority.

The dual-passage heat exchanger tubing, which will be used to model counterflow cooling of the transmission line, has been wound into a 14-inch diameter coil as shown in figure 2.1. After electropolishing and plating, the coil will be instrumented and placed in the experimental chamber.

Radiation heat leak from the model presents a special problem because the temperature of the model varies both temporally and spatially during the cool down.

Conceptually, radiation heat leak could be reduced to a very low level by use of multiple radiation shields along the length of the cable, with each shield held at the same temperature and cooled at the same rate as the section of tubing it surrounds. This approach was judged to be impractical, however, for our spirally-wound model. Instead, we will use a single

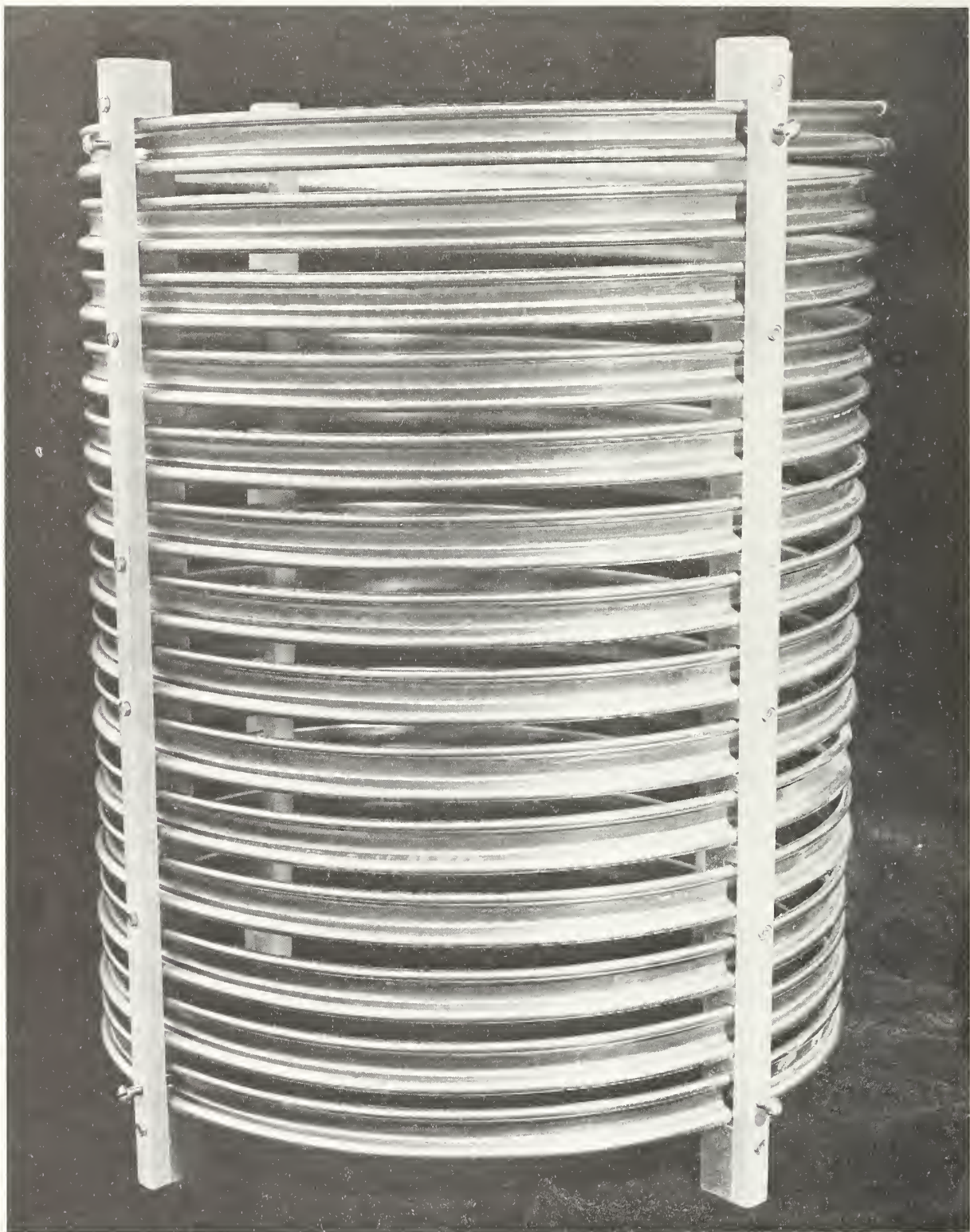


Figure 2.1 Dual passage heat exchange tubing, wound and ready for plating

radiation shield enclosing the entire model. This shield will be held at some spatial average temperature of the model and will be cooled down with the model.

The heat leak can be reduced to about 10 percent of the heat removal rate by 1) reducing the length of the model from 36 m to 18 m, 2) gold-plating the model to reduce its emissivity, 3) wrapping the model with approximately 10 layers of aluminized mylar (too many layers will give too great an uncertainty in the heat capacity) and 4) starting the cool down near 200 K rather than 300 K.

The shortened length of the test section requires a reduced thermal impedance per unit length between the two streams in order to achieve the same value of NTU. Thus, we plan to electro-deposit a 0.002 inch-thick layer of copper beneath the gold layer.

[1] M. C. Jones, Editor, Helium Research In Support of Superconducting Power Transmission, HCP/T6010-01

3.0 COOL-DOWN COMPUTATIONS

The work on numerical calculation of transmission line cool-down is essentially complete and is summarized in the attached paper by M. C. Jones. This paper will be presented at the 71st Annual Meeting of AICHE, Miami Beach, Florida, November 12-16, 1978.

M. C. Jones**

Thermophysical Properties Division
National Bureau of Standards
Boulder, Colorado 80303

ABSTRACT

Numerical solutions of the one-dimensional conservation equations of fluid flow are given for the problem of the cool-down of superconducting power transmission cables. By including the continuity and momentum conservation equations, both time dependent and spatially dependent mass flow may be treated. The equations are applied to specific designs in which one stream of helium fills the bore of a cable while a second fills the space between the outside of the cable and an enclosing pipe. Both co-current flow and counter flow are treated with a variety of boundary conditions. Temperature profiles as a function of time, and total cooldown times are given.

* Work supported by ERDA, Division of Electric Energy Systems and by the Brookhaven National Laboratory, Power Transmission Project.

** Present address: Colorado School of Mines, Chemical and Petroleum-Refining Engineering Department, Golden, CO 80401

Introduction

The successful development and design of Superconducting Power transmission Lines (SPTL's) depends among other things on a thorough knowledge of the fluid mechanics, heat transfer characteristics and thermodynamics of the helium coolant. One problem of particular importance is the initial cool-down of the line from ambient to operating temperature, which is the subject of this paper. This is one of several time-dependent problems, others being the response to a thermal disturbance in an operating line, or the response following a disturbance in the refrigeration system. All are governed by essentially the same set of partial differential equations which are described here.

It is important to develop modeling methods for these problems because the cost of carrying out even small scale laboratory tests is quite considerable. Suitable modeling methods enable the scale-up to full scale apparatus to be made. At the present time, no suitable laboratory results are available for even this, so it is important to make some purely predictive calculations.

A few years ago there were several SPTL development programs active around the world and various cable configurations were suggested. In this paper we consider two such configurations as being representative and reasonably up-to-date. The first is that developed by the Brookhaven National Laboratory (BNL) for an ac, three phase SPTL, the second by the Los Alamos Scientific Laboratory (LASL) for dc. Here we consider two specific designs worked out by these laboratories for economic evaluations of specific applications. In the case of BNL, we give calculations for a design proposed for a 70 km run of a 345 kV, 4800 MVA SPTL. This is for a power transmission corridor under construction by the Long Island Lighting Company (LILCO) in New York connecting a nuclear power plant

on Long Island to a substation near the city. For precise identification, this is referred to as LILCO case III (see reference 1.) For LASL, we performed calculations for a design proposed for an application in Pennsylvania. Evaluations were carried out by the Philadelphia Electric Co. (PECO) for a hypothetical 10,000 MVA transmission corridor between a power station on the Susquehanna River to Philadelphia - a distance of 106 km. We performed calculations on a design submitted by LASL and identified as PECO case C. [2.]

As currently envisaged, SPTL cables are composites of many different materials. In both the LILCO-IIIB and PECO-C designs, hollow core coaxial cables are located inside a stainless steel pipe. In normal operation, coolant flow is through the center of the cables returning, after expansion in a "far-end" turbine expander, in the space between the pipe and the outside of the cables. Moving radially outward, a single coaxial cable consists-at the minimum-of a flexible support helix; conductor tapes or wires plus aluminum or copper stabilizer; dielectric layers; the outer stabilizer and superconductor; a gas-tight shield and/or armor. For a more complete description see references [1,2.] The situation is represented in figure 1. for a 3 phase ac design. The dc case may be thought of as a single such cable inside a pipe.

For the purposes of calculating the cool-down process we have simplified the construction even further, without loss of accuracy and in table 1 we list the compositions assumed in the calculations. Stabilizer and superconductor composite have been lumped to-gether as copper. In the LILCO design, the outer gas seal is a lead sheath, whereas for PECO it is again copper. In table 2, we list the salient dimensions.

In this paper we have calculated the cool-down process for these designs by simultaneous numerical solution of the exact one-dimensional conservation

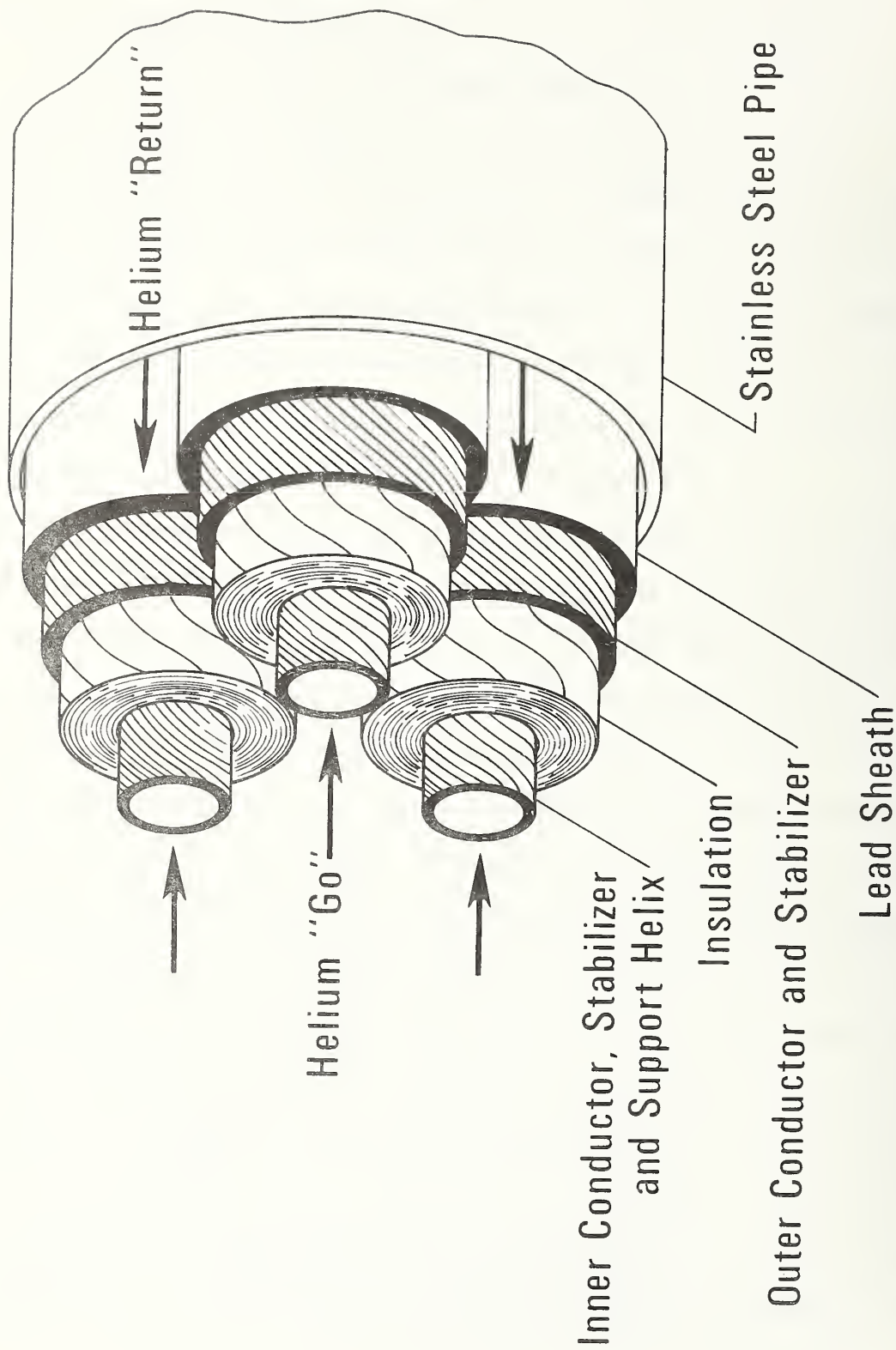


Figure 1. Cut-away view of superconducting power transmission line.

Table 1. Cable compositions used in calculation (kg/m)

	BNL, LILCO-III B.	LASL, PECO-C
Plastic insulation	25.9	4.8
Copper + Superconductor	29.5	6.5
Aluminum	—	—
Stainless steel	26.6	—
Lead	36.2	—
	118.2	11.3
Outer Pipe (Stainless steel)	12.6	2.7
Total mass/m	130.8	14.0

Table 2. cable details (mm.)

	BNL, LILCO-III B	LASL, PECO-C
Inner pipe diameter	50.8	34.0
Outside diameter of cable	135.0	96.8
Inner diameter of insulation	60.2	39.2
Outer diameter of insulation	116.6	84.3
Inside diameter of outer pipe	348.0	110
Distance between refrigeration station, km:	15	6
Assumed steady heat leak from ambient temperature W/m	0.450	0.20
Assumed ideal refrigeration available, MW.	0.80	0.18

equations for the helium streams with appropriate boundary conditions. It did not appear feasible at this time to compute simultaneously the time-dependent radial diffusion of heat through the cable composite, and therefore the cable temperatures at any time and axial position are computed as cross sectional means, i.e., we use a one-dimensional description for these. As will be seen, the results for cooldown-time are probably not sensitive to this assumption.

Previous work on this problem has been of limited extent. For a single coolant stream with constant mass flow, a good value for the cooldown time can be evaluated if the temperature profiles are step-like by an energy balance across the step as proposed by Burke. [3.] If material properties were independent of temperature (decidedly not the case here) the problem is the inverse of packed bed regeneration, and a closed form solution exists. [4.] But again the mass flow rate is assumed uniform and constant. Baron et. al. [5.] presented a numerical method for a single coolant stream for a rigid metal pipe type SPTL. Mass flow rate was not constrained to be constant, but momentum and continuity equations were not solved and therefore the mass flow rate had to be arbitrarily specified. These authors did, however, correctly account for variable helium and pipe properties. Hoffer [6.] has improved on these calculations by determining flow from overall pressure drop, but still assumes uniformity of mass flow. None of the above methods dealt with cooling by two counter-flowing streams which was one of our objectives here.

Analytical Model

The essence of the model is illustrated in Figure 2 where it is seen that the outer pipe, the cable and the two helium streams are each represented by uniform temperature regions for an element of length, dx.

Considering any one of the helium streams we may write down the familiar one-dimensional forms of the mass, energy and momentum conservation equations with pressure P, mean enthalpy H, and mean velocity V as dependent variables

$$\frac{\partial \rho}{\partial t} + \frac{V \partial \rho}{\partial x} + \rho \frac{\partial V}{\partial x} = 0 \quad (1.)$$

$$\rho \frac{\partial}{\partial t} \left(\frac{H+V^2}{2} \right) + \rho \frac{V \partial}{\partial x} \left(\frac{H+V^2}{2} + \Phi \right) = \frac{\partial P}{\partial t} + \Lambda \quad (2.)$$

$$\frac{\partial V}{\partial t} + \frac{V \partial V}{\partial x} = - \frac{1}{\rho} \frac{\partial P}{\partial x} - \frac{fV|V|p}{2a} - \frac{\partial \Phi}{\partial x} \quad (3.)$$

Here, the density ρ is regarded as a known function of P and H, the potential energy Φ is a known function of x, accounting for changes in elevation, and Λ is the heat transfer to the fluid stream per unit length. The friction factor f could be calculated from the local fluid Reynolds no., or, as we have done here, set equal to a constant for typical conditions. p and a are wetted perimeter and cross sectional area of the appropriate helium channel.

There are advantages to retaining P and H as the thermodynamic variables rather than P and T as pointed out by Arp. [7.] In this way we avoid thermodynamic derivatives like specific heat and thermal expansivity which are non-analytic at the critical point and sharply peaked at the transposed critical temperature. The density derivatives in equation (1) can be written in terms of P and H derivatives using the thermodynamic identities

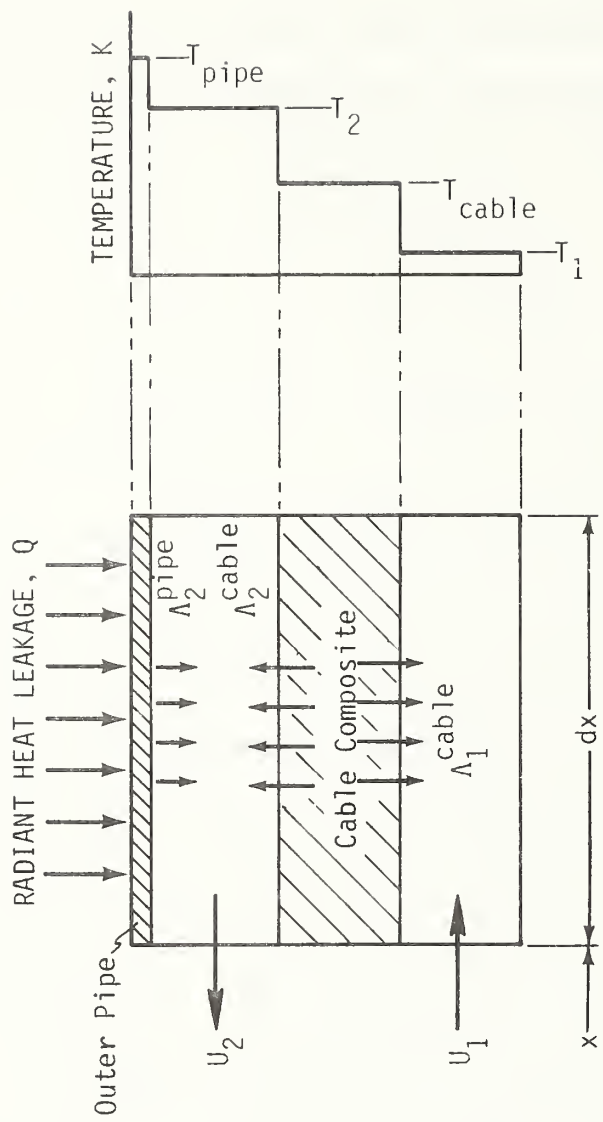


Figure 2. Model for computations

$$d\rho = \left(\frac{\partial \rho}{\partial H} \right)_P dH + \left(\frac{\partial \rho}{\partial P} \right)_H dP \quad (4.)$$

$$\left(\frac{\partial \rho}{\partial H} \right)_P = - \frac{\phi \rho}{c^2} \quad (5.)$$

$$\left(\frac{\partial \rho}{\partial P} \right)_H = \frac{1+\phi}{c^2} \quad (6.)$$

where $\phi = \frac{\rho}{t} \left(\frac{\rho T}{\partial \rho} \right)_s$ - the Gruneisen parameter - and $c^2 = \left(\frac{\partial P}{\partial \rho} \right)_s$, where c is the acoustic velocity. If we then take linear combinations of (1.) (2.) and (3.) we can arrive at a set in which only one time derivative - $\frac{\partial P}{\partial t}$, $\frac{\partial H}{\partial t}$ or $\frac{\partial V}{\partial t}$ - occurs in each equation, this form being preferable for numerical solution. The resulting set - equation (3.) being unchanged as equation (9.) - is

$$\frac{\partial P}{\partial t} = V \frac{\partial P}{\partial x} - \rho c^2 \frac{\partial V}{\partial x} + \phi \left[\frac{\Lambda}{a} + \frac{\rho V^2 f |V| P}{2a} \right] \quad (7.)$$

$$\frac{\partial H}{\partial t} = - V \frac{\partial H}{\partial x} - c^2 \frac{\partial V}{\partial x} + \frac{1+\phi}{\rho} \left[\frac{\Lambda}{a} + \frac{\rho V^2 f |V| P}{2a} \right] \quad (8.)$$

$$\frac{\partial V}{\partial t} = - \frac{1}{\rho} \frac{\partial P}{\partial x} - V \frac{\partial V}{\partial x} - f \frac{V |V| P}{2a} - \frac{\partial \phi}{\partial x} \quad (9.)$$

There is one such set of three equations for each fluid stream and the independent variables and coefficients can be subscripted 1 and 2 for the inner and outer streams respectively. They are coupled to appropriate energy equations for the cable and outer pipe through the heat transfer terms Λ_1 , and Λ_2 .

For the cable composite the appropriate one-dimensional energy conservation equation is of the form

$$\sum \rho_i C_i a_i \frac{\partial T_{\text{cable}}}{\partial t} = \sum \frac{\partial}{\partial x} \left(k_i a_i \frac{\partial T_{\text{cable}}}{\partial x} \right) - \Lambda_1^{\text{cable}} - \Lambda_2^{\text{cable}} \quad (10.)$$

where ρ_i , C_i , k_i and a_i are the density, specific heat, thermal conductivity and cross sectional area of the i^{th} cable component. It is easy to show that the heat conduction term on the right hand side is quite negligible in all cases considered. A similar equation can be written for the outer pipe

$$(\rho C a)_{\text{pipe}} \frac{\partial T}{\partial t} = \frac{\partial}{\partial x} \left[(k a)_{\text{pipe}} \frac{\partial T}{\partial x} \right] + Q - \Lambda_2^{\text{pipe}} \quad (11.)$$

where again for practical purposes the first term on the right hand side can be neglected. Q is the radiant heat leakage per unit length to the outer pipe from the ambient temperature vacuum pipe (not shown in figures 1 and 2) through a multilayer insulation which is assumed to cover the outer pipe. In the computations it is given a simple $(T_{\text{ambient}}^4 - T_{\text{pipe}}^4)$ dependence.

In the equations (7.) and (8.) written respectively for stream 1 and stream 2 the heat transfer terms may be written

$$\Lambda_1 = \Lambda_1^{\text{cable}} \quad (12.)$$

$$\Lambda_2 = \Lambda_2^{\text{cable}} + \Lambda_2^{\text{pipe}} \quad (13.)$$

In the absence of numerical evaluations of the radial diffusion of heat to determine Λ_1^{cable} and Λ_2^{cable} we are forced to adopt a fairly crude model.

Since the thermal conductance through the cable is typically an order of magnitude smaller than the fluid film conductance, the latter is assumed to be infinite and we assume these terms are proportional to the difference between the mean cable temperature and the appropriate fluid stream temperature. Thus

$$\Lambda_1^{\text{cable}} = p_1 h_1 (T_{\text{cable}} - T_1) \quad (14.)$$

$$\Lambda_2^{\text{cable}} = p_2 h_2 (T_{\text{cable}} - T_2) \quad (15.)$$

where

$$h_1 = \frac{k}{r_1} / \ln \left(\frac{\bar{r}}{r_1} \right) \text{ and } h_2 = \frac{k}{r_2} / \ln \left(\frac{r_2}{\bar{r}} \right) \quad (16.)$$

and r_1 , and r_2 are the inner and outer radii of the plastic insulation, \bar{r} the mean radius and k the thermal conductivity of the insulation evaluated at T_{cable} . In other words, we compute the conductances h_1 , and h_2 as steady state values. In fact, for the transient cooling of a slab, following a step change in temperature a linear heat transfer relationship for the average slab temperature is approached after about 2 time constants, this being given by δ^2/α where α is the thermal diffusivity and δ the slab half-thickness. For the cases considered here, this time constant is of the order of 10^3 seconds at room temperature and 10^2 seconds at operating temperature, so the approximation should be good whenever the active cooling period greatly exceed this. The sensitivity of the results to this approximation is discussed further below.

Finally for the term Λ_2^{pipe} in (11) and (13) we use an average heat transfer coefficient, h_3 , for turbulent flow with Reynolds number based on a

mean hydraulic diameter

$$\Lambda_2^{\text{pipe}} = p_3 h_3 (T_{\text{pipe}} - T_2) \quad (17.)$$

In addition to the above set of equations, boundary conditions must be specified appropriate to the particular mode of cooldown being used. We have investigated the following modes. Co-current flow through cable cores and the space between cables and outer pipe; counterflow with return stream expanded down to lower pressure at fixed isentropic efficiency (far-end expander); counterflow with return stream refrigerated to specified thermodynamic state (far-end refrigerator). For all cases, since the heat conduction terms of (10) and (11) have been neglected, no boundary conditions were needed for either T_{cable} or T_{pipe} . For the set of equations (7.), (8.) and (9.) applied to each stream, we need three boundary conditions, but note that they may be at different ends of the cable ($x = 0$ and $x = L$) and, further, we may have two conditions on one dependent variable, one on a second and none on a third. The alternatives are displayed in table 3. In some cases, such as H , at $x = 0$, an explicit time dependence is given, while in other cases such as H_2 and V_2 at $x = L$, one dependent variable is expressed as a function of others.

For initial conditions the entire system was assumed to be at ambient temperature with a steady state velocity and pressure profile specified.

Material Properties

In equations (7.)-(9.) the coefficients ρ , c^2 , ϕ and, through Λ , T are to be regarded as known functions of the dependent variables P and H . For

Table 3. Boundary Condition Types

	(i) Co-current, constant pressure (prop)		(ii) Co-current flow		(iii) Counterflow, Far-end refrigerator		(iv) Counter flow, Far-end expander	
	$x=0$	$x=L$	$x=0$	$x=L$	$x=0$	$x=L$	$x=0$	$x=L$
P_1	constant	constant	constant	—	constant	constant	constant	constant
H_1	$H_1(t)$	—	$H_1(t)$	—	$H_1(t)$	—	$H_1(t)$	—
V_1	—	—	—	const./ $\rho_1(H_1, P_1)$	—	—	—	—
P_2	constant	constant	—	constant	constant	—	constant	—
H_2	$H_2=H_1$	—	$H_2=H_1$	—	—	$H_2(t)$	—	$H_2=H_2(P_1, P_2, H_1)$
V_2	—	—	const./ $\rho_2(H_2, P_2)$	—	—	$\rho_2(H_2, P_2)V_2 = \rho_1(H_1, P_1)V_1$	$\rho_2(H_2, P_2)V_2 = \rho_1(H_1, P_1)V_1$	—

fast computer evaluation it was found advantageous to express these as polynomials. These were fitted to the more exact data derived from the equation of state of McCarty in the range 0.3 - 2.0 MPa and 4 to 300K. For ρ the average error was $\pm 0.5\%$ or less at higher temperatures with a maximum of 1.7% near the transposed critical state. For c^2 the average error was $\pm 2\%$ for $P < 1.2$ MPa and 3% for $1.2 < P < 2.0$ MPa. The average error in ϕ was -3% or less for $P > 0.5$ MPa and +6% for $P < 0.5$ MPa. Finally, temperature error averaged ± 0.05 K for $P > 0.4$ MPa, and ± 0.1 K for $0.3 < P < 0.4$ with a maximum error of 0.2K occurring near transposed critical states. The functions $c^2(P,H)$ and $\phi(P,H)$ are shown plotted in figure 3.

In equations (10.) and (11.) it is assumed first that the specific heats C_i of the cable components are available as functions of temperature (T_{cable} or T_{pipe}). Simple expressions were again fitted to selected data from the literature [9, 10, 11, 12] for fast computer evaluation and these are illustrated in figure 4 for polycarbonate, copper, lead and stainless steel. These fits are generally better than $\pm 5\%$.

Perhaps the most important property is the thermal conductivity of the plastic insulation needed in equation (16.) This is not a simple property to measure experimentally because in fact the insulation consists of many layers of thin tape wound under tension and, in operation, impregnated with helium. Our calculations were based on measurements [1.] of the thermal conductivity of four layers of 75 μm polycarbonate in the presence of helium gas at about 0.5 MPa pressure. Polycarbonate is a candidate insulation with high density polyethylene and polysulphone. Pressure was shown to increase the effective thermal conductivity of the layers but appeared to have reached a limit for polycarbonate at about this pressure. Thermal conductivities

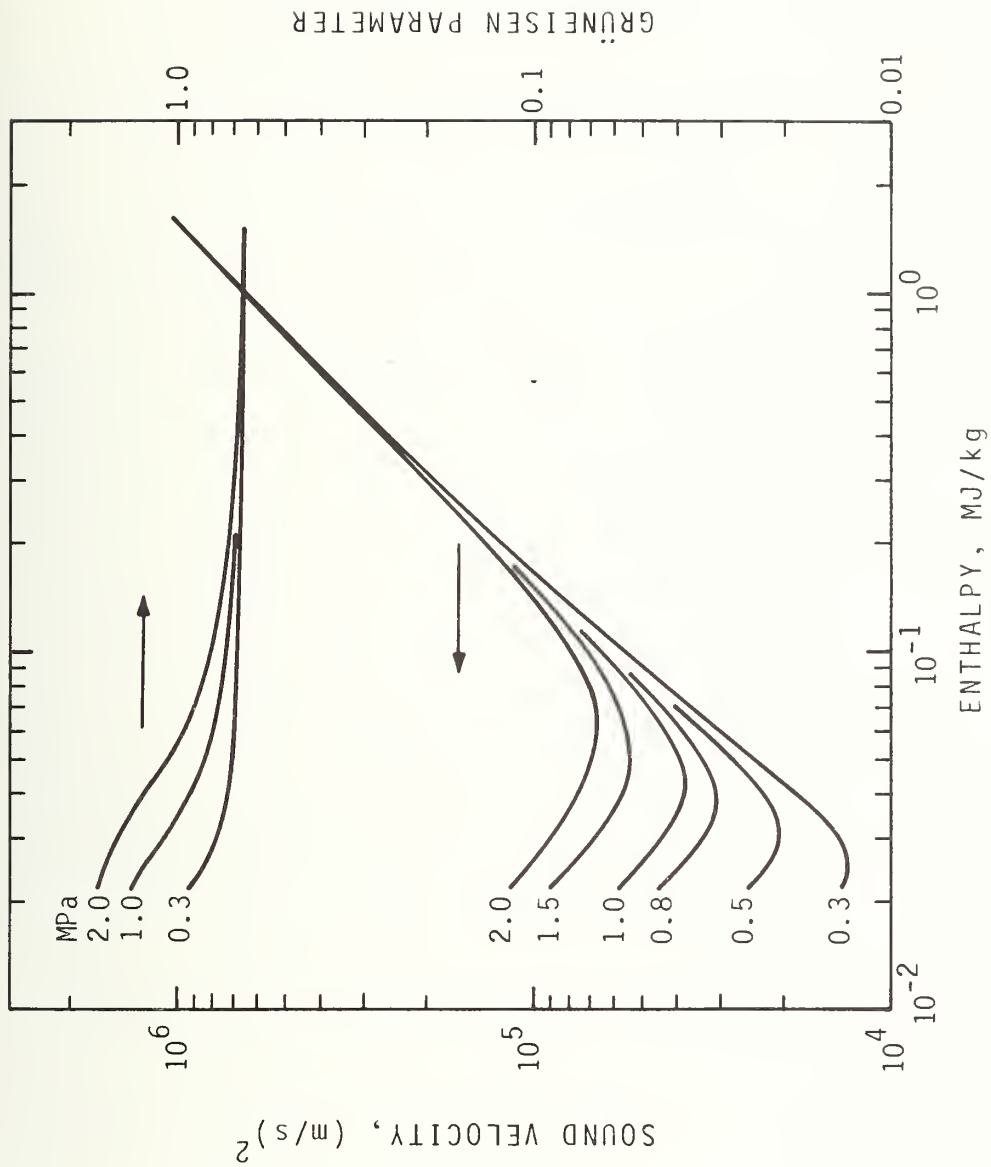


Figure 3. The functions $c^2(P,H)$ and $\phi(P,H)$

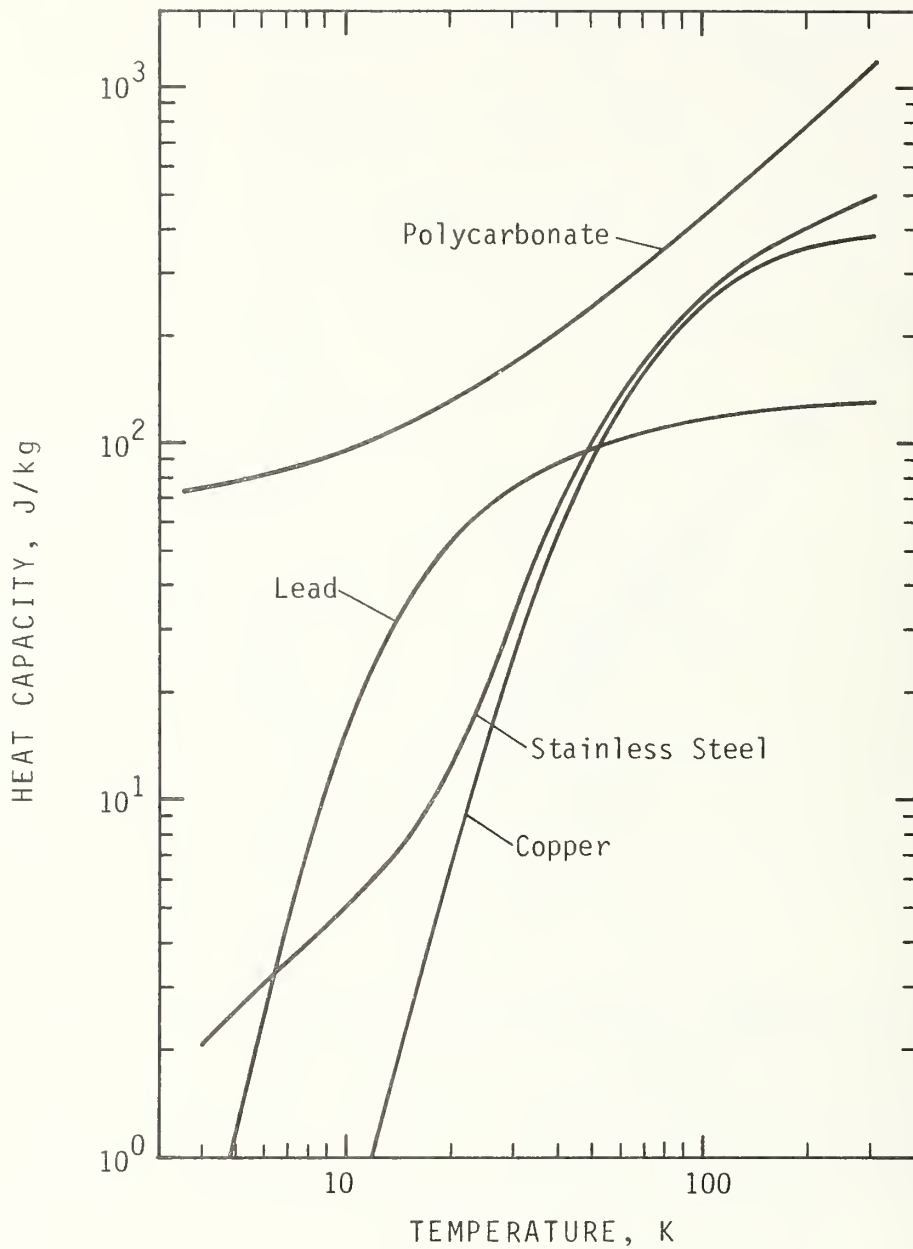


Figure 4. Heat capacities of cable components; the functions $C_i(T)$

were measured at 4.2, 20, 100, and 300K. Unfortunately, a sharp increase takes place between 100 and 300K and therefore, although we could fit a polynomial to these data quite accurately, the actual form of the temperature dependence between these two temperatures is unknown, and the fitted curve shown in figure 5 must be regarded as rather approximate.

Numerical Method.

Integration of the set of eight partial differential equations was accomplished using the computer program PDECOL developed by Madsen and Sincovec. [13] This program is based on the method of lines and uses finite element collocation for the discretization of the spatial variable. Using piecewise polynomials for the trial function space, the procedure reduces the system to a set of first order ordinary differential equations with time as the independent variable. The program then uses established procedures for stiff systems to perform the time integration. PDECOL has been tested by its authors and found to be up to an order of magnitude faster than a similar finite difference technique for the same accuracy.

Since PDECOL was designed for non-linear partial differential equations it was relatively straightforward to introduce a properties subroutine to calculate the properties discussed above for every new value of the solution vector and supply the solution dependent coefficients in the differential equations. This adds significantly to the run time, but was still less than 10% in our computations.

Results of Computations.

There are essentially two schemes which may be used to cool a SPTL down. In the first, cold helium gas from a refrigerator enters the cable cores and the outside space between cables and enclosing pipe in co-current flow.

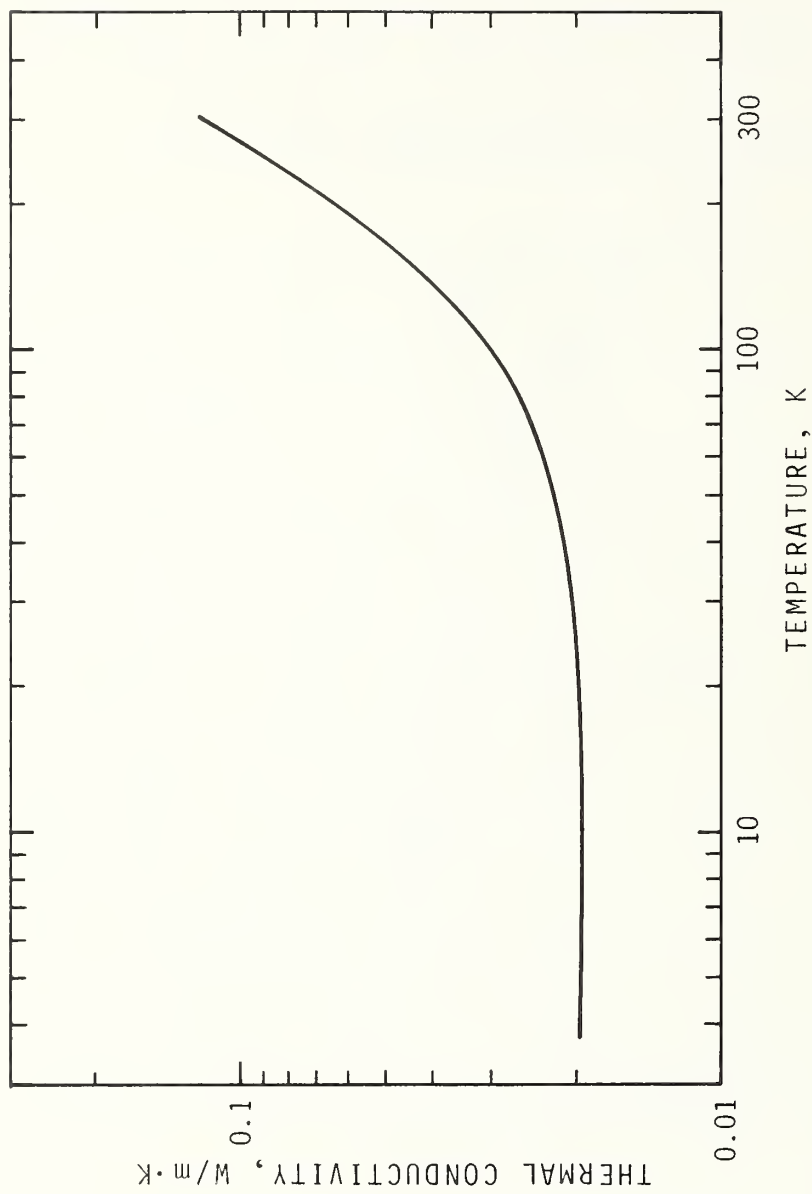


Figure 5. Thermal conductivity of helium impregnated polycarbonate layers

The cooldown time of the refrigerator is likely to be a few hours compared to days for the transmission line, so for most of the cooldown period the refrigerator, in this mode of cool-down, receives return helium gas or fresh make-up gas at ambient temperature and supplies gas at the coldest temperature operating much as a liquifier. In the second scheme, the refrigerator supplies only the cable cores and at the far end the helium is either re-refrigerated or expanded to produce more refrigeration prior to being returned in counter-flow in the outside space. Because of the great length, the cable behaves as a highly effective counterflow heat exchanger, despite the poor conductivity of the insulation, so in this case cooldown takes much longer for a given mass flow. On the other hand, no storage or return piping is needed. A further advantage of this second scheme is that temperature stress is much reduced both axially and radially.

We have calculated cooldown of the cable designs described for both the co-current flow and counterflow alternatives and we find that the cooldown time is limited in two different ways. In co-current flow, cool-down proceeds very rapidly and is only limited by the capacity of the refrigerator to supply the cable with helium. Therefore, in these calculations a constant total mass flow rate was maintained from start to finish. In counterflow cooling, because of the inherently greater duration of the process, it was found that much higher mass flow could profitably be used, and that the rate of cool-down was limited by the permissible pressure drop. These calculations were therefore done with a constant pressure drop, and so the mass flow necessarily increased during the course of cooldown.

As an example of co-current cooling, we give results from a computation for the LASL/PECO cable design (6 km length) in figures 6 and 7. In this

example, most of the mass flow was in the outer space. After an initial transient, during which inlet temperature was lowered to 10 K with a time constant of 2.8 hours, the total mass flow at inlet was held at 25 g/s. The mass flow profiles of figure 6 show a non-uniformity as the cable free space is filled with dense fluid from the left. Figure 7 shows the corresponding cable temperatures, complete cooldown occurring in 75 hours. After the initial transient, the ideal refrigeration was steady at 0.15×10^6 W which is a shade less than what is expected to be available during cooldown for this case. Available refrigeration is based on steady state loads and the need for a standby machine. Both machines would be available during cooldown.

A similar calculation was performed for the BNL/LILCO design. Mass flow rate was 129 g/s with a near uniform pressure of 1.52 MPa, and the time constant for the initial lowering of the temperature 28 hours. The ideal refrigeration power, 0.75×10^6 W, is again just inside the 0.8×10^6 W expected to be available. Because of time limitations, this calculation was terminated after cooldown was about 1/2 complete. However, at this point the cold front was moving at a constant velocity of 33.2 meters per hour and so the total cooldown time can be confidently estimated to be 472 hours. (19.7 days)

For both of the above calculations, boundary conditions were of type (ii). It was found that a solution could only be obtained if mass flow and pressure were fixed at opposite ends. Further, if mass flow in the outer space were fixed at inlet, the mass flow in the core had to be fixed at outlet, otherwise, to conserve mass, the solution sometimes called for a warm gas inflow from the far end. This was true for small mass flow rates in the cores which, when fixed at the cold inlet were insufficient to fill the core at the rate dictated by heat transfer to the outer stream.

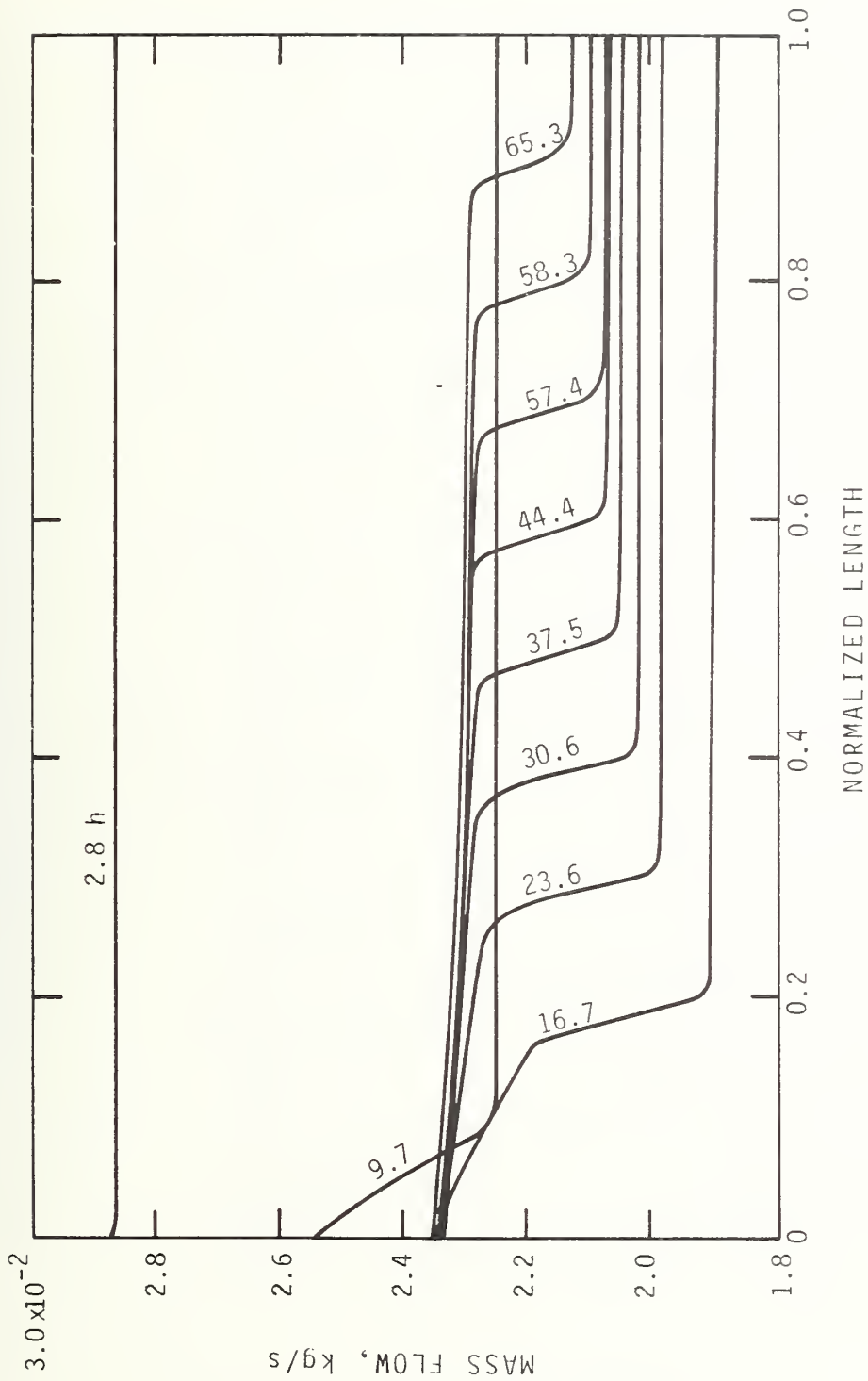


Figure 6. Mass flow profiles for cooldown of the L1SL/PECO design using co-current flow of the helium streams. These profiles are for flow in the space outside the cable. Flow in the core was an additional 1 g/s held constant at outlet.

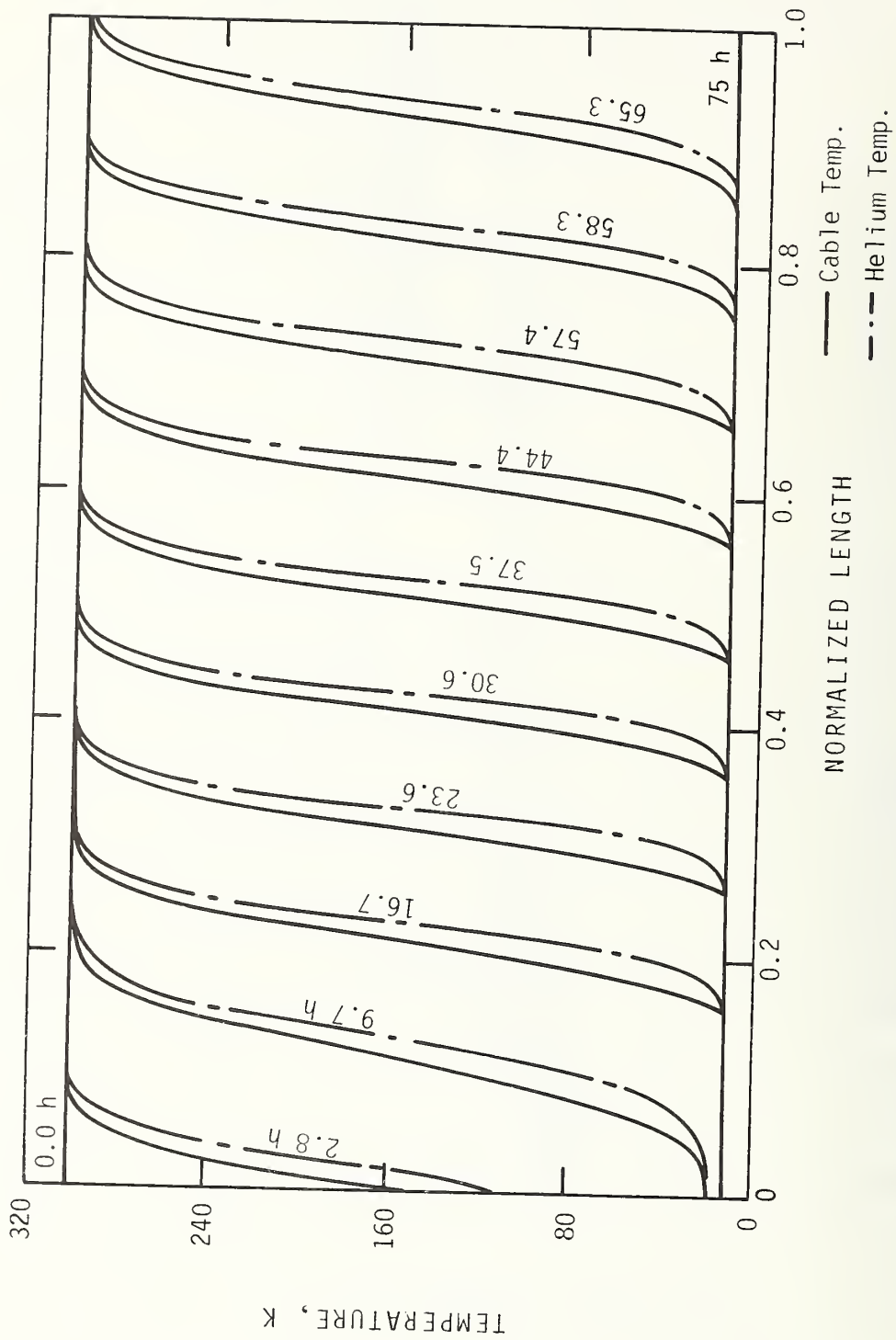


Figure 7. Temperature profiles for the cable and the outside helium stream.

To illustrate counterflow cooling, we show results for the BNL/LILCO design in figures 8 and 9. In the case shown, two refrigerator stations were assumed to supply helium at 10 K to the core and outer space, respectively, at the near and far ends of 15 km length of cable. Boundary conditions were of type (iii). Using a pressure of 1.5 MPa at the first refrigerator, pressure drop in the cores was held at 1.0 MPa, while at the far-end the emerging mass flow was assumed to pass to the second refrigerator station, re-entering the cable again in the outer space. Specification of the pressure of the return stream at the first refrigerator station completes the boundary conditions. Runs were made with both 1.5 MPa and 0.5 MPa for this pressure with only marginal differences in the resulting cooldown time. The cooldown time was 20.5 days. The ideal refrigeration powers for the two refrigerators were of course variable and are plotted in figure 9 as a function of time as is also the mass flow (in this case it was essentially uniform in the spatial dimension).

The importance of this calculation for the BNL/LILCO design is that it is probably the fastest possible cooldown using the counterflow mode. In fact it is not planned to position a refrigerator at the far-end, but only an expander. Here we run into the difficulty that in order to obtain a high mass flow for rapid cooldown, pressure drop in the cable cores is at the expense of available expansion. As an example, we ran a calculation for BNL/LILCO where the helium from the refrigerator entered the cable cores at 1.5 MPa with 0.8 MPa pressure drop. With 5.0 MPa specified for the helium return pressure at the refrigerator this left an expander pressure ratio of only 1.09. Thus the expander, with an assumed isentropic efficiency of 75%, contributed very little refrigeration and the cooldown time was 58 days. We do not feel that much improvement in the cooldown time can be obtained by this method.

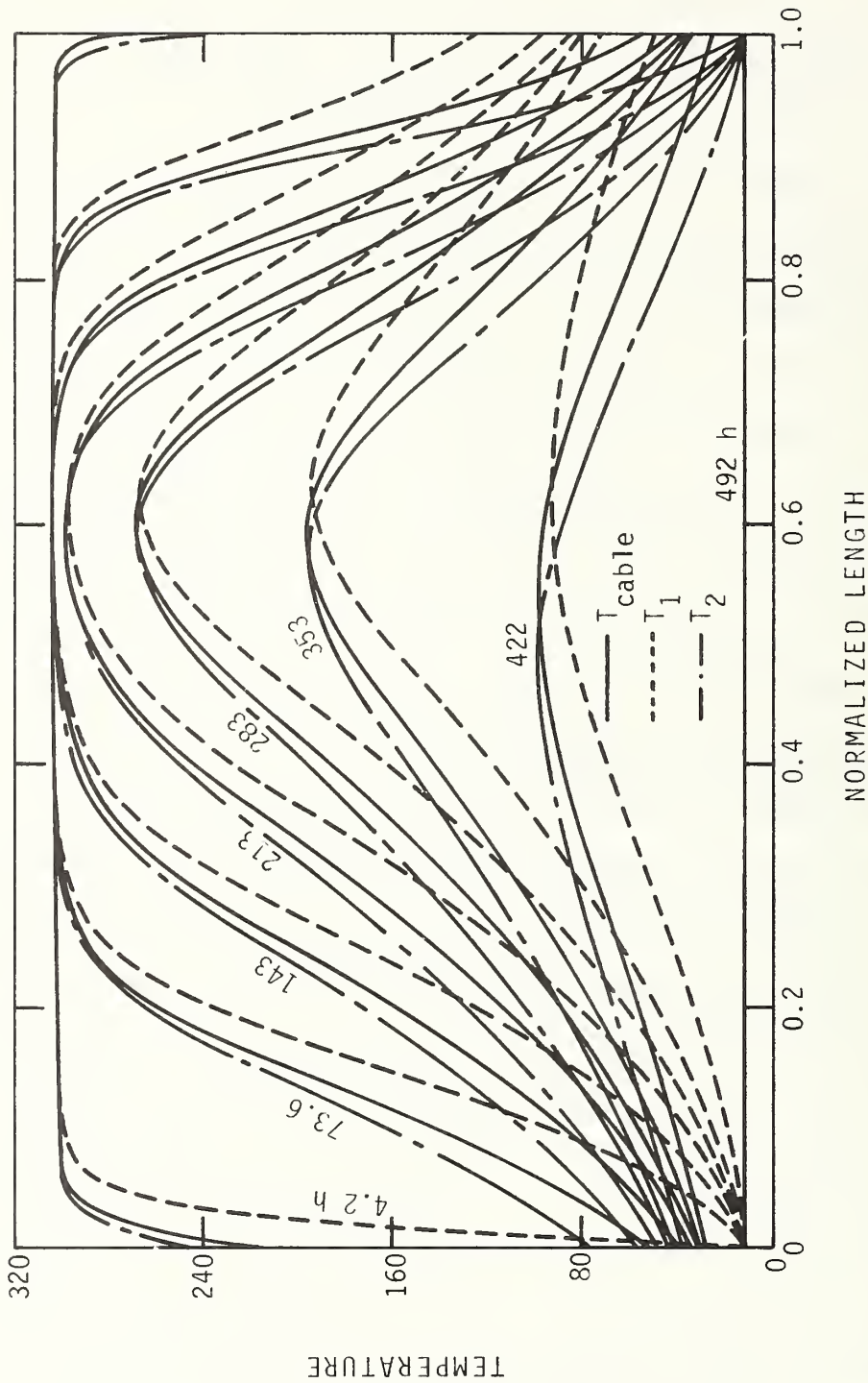


Figure 8. Temperature profiles for cooldown of the BNL/LILCO design with counterflow of the helium streams. It is assumed that refrigerators are positioned at both ends of the cable supplying, respectively, the cores and outside space with helium at 10 K.

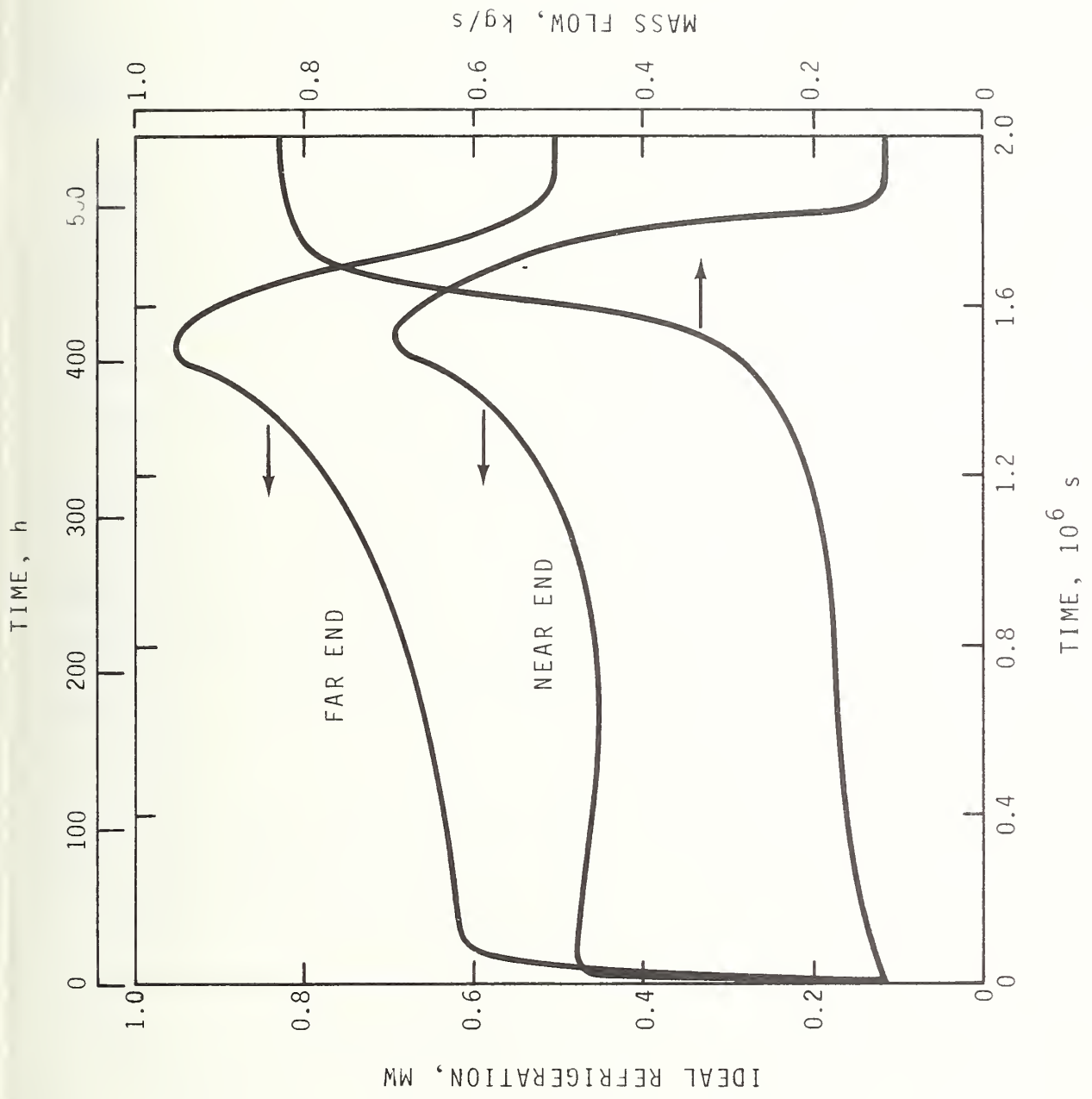


Figure 9. Plots of ideal refrigerator power and mass flow of helium at inlet to the cores vs. time, for the BNL/LILCO case with counter-flow of the helium streams.

The corresponding case for counterflow cooling of the LASL/PECO design using a similar far-end expansion resulted in a cooldown time of 7.0 days when the pressure drop in the cold core was held constant at 0.5 MPa. This is, however, not the fastest possible case as the core pressure drop is still relatively small. However, we have not determined the optimum distribution of pressure drop between cable core and expander.

A final point concerns all of the calculations: in order to obtain stable flow it was found necessary to lower the inlet helium enthalpy continuously with time until the desired inlet temperature was reached and to take a small pressure drop across an upstream restriction. Failure to do this led to flow reversals and pressure pulsations in the solution with excessive computational time. Thus, the constant inlet pressure actually refers to pressure upstream of the restriction. In view of the fact that in experiments such pulsations are common we believe this to be physical and not an artifact of the calculation. In all calculations we have taken $\Delta P_{\text{restriction}} / \rho V^2 = 15$, and the inlet enthalpy reduced linearly to its constant value in either 10^4 or 10^5 seconds.

Discussion of the Results.

The first part of this discussion is concerned with the validity of the cooldown results predicted by the model and the integration procedure used. First of all, the number of collocation points and the desired local relative error to be maintained during the integrations were arrived at by preliminary single stream calculations on a simple pipe with constant properties and constant coolant mass flow. This problem has an exact solution [4]. For long pipes, Shutt [14] arrived at a simple asymptotic expression for cooldown time. For 202 and 102 collocation points our calculations of cooldown time were within 0.3% and 1.3% respectively when the local relative error was held at 0.1%. All calculations reported above were performed with 102 collocation

points and relative error 0.1%. Therefore we believe our numerical errors on cooldown time to also be of the order of 1%. In any counter-flow calculation, on the other hand, the error should be smaller because cooldown is more gradual and solutions are less sharply varying in the x direction.

Of the approximations made in the model we believe only the pseudo-steady-state heat transfer resistance across the cable insulation to be weak, and then only for co-current calculations which involve the most rapid cooldown. For a single stream and pipe with constant properties, Shutt has shown that when the width of the active cooldown zone is small compared to the pipe length the cooldown time is independent of the heat transfer coefficient. This is certainly the case for the co-current runs reported here as seen in figure 7, for example. To verify this we ran the calculations from which this figure is taken with the thermal resistance arbitrarily doubled. No significant change in cooldown time resulted. Therefore we believe that our computed cooldown times are reliable. Furthermore, through considerable experience in running these cooldown problems and other transient helium flow and heat transfer problems at this laboratory, we feel that the combination of the differential equation set as formulated here and the computational package PDECOL has considerable potential as a modeling tool. It has shown itself to be both flexible and robust, capable of handling flow reversals and pressure wave propagation in addition to the slower density wave propagation characteristic of cooldown.

We now consider the practical results of these calculations. Certainly co-current flow is the fastest cooldown mode. Were it not for the fact that in this mode one is limited by available refrigeration, even faster cooldown could be achieved. (For example, calculations were made on LASL/PECO with, first, a fixed pressure drop of 1.2 MPa until the flow rate reached 200 g/s. Thereafter the flow rate was held constant at this value. The resulting cooldown time was 17 hours.

But required ideal refrigeration capacity was 1.2 MW -- at least a factor of six higher than would be available.)

For counterflow cooling, the 7 days (a conservative estimate) computed for LASL/PECO using a far-end expander is certainly an acceptable time and this would be an attractive cooldown mode, being essentially the same operating mode as for steady state operation. On the other hand, we have only been able to broadly bracket cooldown time for BNL/LILCO. The one certainty is that it will be hard to beat the 20.5 day cooldown time computed using a far-end refrigerator. Some investment will have to be made to achieve this time: either the cost of a mobile refrigeration unit for such temporary duty, or the use, say, of liquid nitrogen in a heat exchanger at the far-end, or, as shown above we could fall back on the co-current mode, which gave 19.7 days cooldown time but which requires a separate warm gas return line. Yet another possibility, which may avoid further investment, however, is to evacuate the outer space, supply helium to two cable cores using the third as a warm gas return. In this way the thermal coupling between streams should be greatly reduced allowing cooldown to proceed up the first two cables and down the third as with a single stream or the co-current flow examples discussed above. Since in this mode pressure drop will not be a limitation there is no reason why the full capacity of available refrigeration should not be used and a cooldown time of about 20 days should be attainable.

Conclusions

1. The formulation of the transient flow equations with P, H and V as dependent variables, together with the numerical partial differential equation package PDECOL of Madsen and Sincovec provides a powerful, accurate, and flexible tool for transient single phase variable property flow calculations, particularly with coupled streams.

2. Cooldown for specific SPTL Designs was investigated with a reasonably detailed description of the cable construction from the standpoint of thermal capacity. Realistic estimates of cooldown times were made for a variety of different operating modes.

Acknowledgments

Helpful discussions with Neil Madsen of the Lawrence Livermore Laboratory on the use of PDECOL allowed the author to do things that it was not originally designed for. His guidance and patience was greatly appreciated.

Vincent Arp of the National Bureau of Standards showed his customary helpful interest and contributed the polynomial fits for helium properties.

References.

1. Power Transmission Project-Progress through Fiscal Year 1976. Report PTP#69, BNL 22202. Brookhaven National Laboratory December 27, 1976.
2. Details are given in internal reports of the Los Alamos Scientific Laboratory (1976) and are available on request from F. J. Edeskuty.
3. Burke, J. C., Byrnes, R., Post, A. R., and Russia, F. E. Advances in Cryogenic Engineering, vol. 4 (Plenum Press, New York, 1960) p 378.
4. Carslaw, H. S. and Jaeger, J. C. Conduction of Heat in Solids, Second Edition. (Oxford University Press, 1959)
5. Baron, A. M., Eroshenko, V. M., Yaskin, L. A. Cryogenics (1977)
6. Hoffer, J. K. private communication, see reference 2.
7. Arp, V. D. Cryogenics 15, 285 (1975)
8. McCarty, R. D., J. Phys. Chem. Ref. Data 2, 923 (1973)
9. Schramm, R. E., Clark, A. F., and Reed, R. P. NBS Monograph 132. (U.S. Dept. of Commerce, National Bureau of Standards, 1973)
10. Miller, A. P. and Brockhouse, B. N. Can. J. Phys. 49, 704 (1971)
11. Collings, E. W., Jelinek, F. J., Ho, J. C. and Mathur, M. P. Advances in Cryogenic Engineering vol 22 (Plenum Press, New York, 1977) p 159.
12. Corruccini, R. J. and Gniewek, J. J. NBS Monograph 21 (U.S. Dept. of Commerce, National Bureau of Standards, 1960)
13. Madsen, N. K., and Sincovec, R. F. in Numerical Methods for Differential Systems, L. Lapidus and W. E. Schiesser, editors, (Academic Press, Inc New York, 1976.)
14. Shutt, R. P. Internal report of the Brookhaven National Laboratory, (1976) available on request.

U.S. DEPT. OF COMM. BIBLIOGRAPHIC DATA SHEET	1. PUBLICATION OR REPORT NO. NBSIR 79-1618	2. Gov't Accession No.	3. Recipient's Accession No.	
4. TITLE AND SUBTITLE HELIUM RESEARCH IN SUPPORT OF SUPERCONDUCTING POWER TRANSMISSION		5. Publication Date October 1979	6. Performing Organization Code	
7. AUTHOR(S) David E. Daney	8. Performing Organ. Report No.			
9. PERFORMING ORGANIZATION NAME AND ADDRESS NATIONAL BUREAU OF STANDARDS DEPARTMENT OF COMMERCE WASHINGTON, DC 20234		10. Project/Task/Work Unit No.	11. Contract/Grant No. 433475-S	
12. SPONSORING ORGANIZATION NAME AND COMPLETE ADDRESS (Street, City, State, ZIP) Brookhaven National Laboratory Upton, New York 11973		13. Type of Report & Period Covered Interim/FY 78	14. Sponsoring Agency Code	
15. SUPPLEMENTARY NOTES <input type="checkbox"/> Document describes a computer program; SF-185, FIPS Software Summary, is attached.				
16. ABSTRACT (A 200-word or less factual summary of most significant information. If document includes a significant bibliography or literature survey, mention it here.) During FY 78, the NBS Thermophysical Properties Division program of supporting research for Superconducting Power Transmission Line (SPTL) development focused on three tasks: 1) Numerical computation of SPTL cool down by both single stream and counter flow methods. 2) Experimental modeling of counterflow SPTL cool down. 3) Thermal cycling of lengths of lead-sheathed model cable destined for testing in the BNL 5th Ave. facility. The preparation of computer codes and numerical computation of SPTL cool down were completed and the results are given in Section 3. These calculations confirm our original intuitive judgment that cool-down times for the counterflow arrangement can be long--twenty days or more. Greater than anticipated computer run times and costs required a reduction of effort on experimental modeling of counterflow cool down. Consequently, completion of this task will be delayed until FY 79. Two sections of cable underwent extensive thermal cycling, and the results of these tests are given in Section 1. The complex structure of the cable leads to unusual (although reproducible) load vs time curves. Funding limitations required postponement until FY 79 of the experimental evaluation of heat flow sensors as a means of non-intrusive vacuum indication for SPTL vacuum envelopes. This task together with experimental modeling of cool down will form the heart of our program in FY 79.				
17. KEY WORDS (six to twelve entries; alphabetical order; capitalize only the first letter of the first key word unless a proper name; separated by semicolons) Cable cool-down; cool-down helium; liquid helium; superconducting power transmission, thermal cycling, thermal stress.				
18. AVAILABILITY <input checked="" type="checkbox"/> Unlimited <input type="checkbox"/> For Official Distribution. Do Not Release to NTIS <input type="checkbox"/> Order From Sup. of Doc., U.S. Government Printing Office, Washington, DC 20402, SD Stock No. SN003-003- <input checked="" type="checkbox"/> Order From National Technical Information Service (NTIS), Springfield, VA, 22161	19. SECURITY CLASS (THIS REPORT) UNCLASSIFIED	21. NO. OF PRINTED PAGES 64	20. SECURITY CLASS (THIS PAGE) UNCLASSIFIED	22. Price \$4.50

MSK 71-1010